Slip-stuck kinematics of fault surfaces in laboratory experiments: implications for heterogeneous slip distributions during earthquake events

Uddalak Biswas[1,2], Manaska Mukhopadhyay[1], Nibir Mandal[1*]

[1]Department of Geological Sciences, Jadavpur University, Kolkata, India
[2]Department of Earth Sciences, Indian Institute of Engineering Science and Technology, Shibpur, Howrah, West Bengal, India
uddalakbiswashriku@gmail.com (U. Biswas), manaska.geos@gmail.com (M. Mukhopadhyay), * nibir.mandal@jadavpuruniversity.in (N. Mandal)

This manuscript has been submitted for publication in the ***International Journal of Rock Mechanics and Mining Sciences (IJRMMS)***. Please note that the manuscript has not undergone any peer-review process and is currently under review. Subsequent versions of this manuscript may have slightly different content. If accepted, the final version of this manuscript will be available via a link on this webpage. Please feel free to contact any of the authors if you have questions or feedback.

Slip-stuck kinematics of fault surfaces in laboratory experiments: implications for heterogeneous slip distributions during earthquake events

Uddalak Biswas[1,2], Manaska Mukhopadhyay[1], Nibir Mandal[1]*

[1]Department of Geological Sciences, Jadavpur University, Kolkata, India
[2]Department of Earth Sciences, Indian Institute of Engineering Science and Technology, Shibpur, Howrah, West Bengal, India

AIRTICLE INFO

Keywords:
Fault surface roughness
Slickensides lineation
Slip heterogeneity
Analogue experiments
Shear surface simulations
Anisotropic fractal dimensions

Highlights:

• Roughness mapping reveals heterogeneous slip localization on shear surfaces.
• Isotropic (stick zone) and anisotropic (slip zone) roughness domains are mapped.
• Stuck and slip zones display characteristic shear surface irregularity patterns.
• In experiments shear-surface orientation decides the degree of slip heterogeneity.
• Stuck- and slip-zone roughness yields distinctive directional fractal dimensions.

ABSTRACT

Combining field observations with analogue laboratory experiments, this study aims to use surface-roughness characteristics as an indicator of the heterogeneous slip partitioning along shear surfaces. We investigated the roughness of shear surfaces in sheared quartzite of the Singhbhum Shear Zone, eastern India, and identified two distinct kinematic domains: slip zone and stick zone, marked by strong and weak or no roughness anisotropy, respectively. The experiments, run on brittle-ductile models under a pure shear condition suggest the initial inclination (θ) of shear fractures to the compression direction as a crucial factor in determining their competitive development (measured in terms of their relative area coverage) on the shear surface. Using a laser profilometer we constructed 3D topologies of both field and experimental shear surfaces, which are presented to show their distinctive roughness characteristics. The slip and stick zones differ from each other in the fractal properties of their surface irregularities. ΔD [difference between across- ($D_{\perp}$) and along- ($D_{\parallel}$) slip direction] is calculated to evaluate the degree of roughness anisotropy. This fractal parameter indicates strong anisotropy in slip (ΔD = 0.0787 – 0.2118) zones, which is virtually absent in stick zones (ΔD = 0.0024 – 0.0603). We thus propose ΔD as an effective parameter to delineate the slip and stick zones on a shear surface. Finally, the article presents an in-depth discussion of the geological implications, e.g., earthquake event patterns of this slip-stick roughness study.

1. Introduction

Faults in the upper brittle crust accommodate large displacements, which localize preferentially in discrete slip zones on the fault surfaces (Brodsky et al., 2011; Chester et al., 2004; Cowan et al., 2003; Sibson, 1977). The spatial distribution of slip zones on a seismic fault provides the most crucial information required to interpret the faulting process (Wells and Coppersmith, 1994) and rupture propagation dynamics (Scholz, 2002) of sizeable earthquake events in a tectonically active region. The geometrical characteristics of slip zones, such as their size, distribution and roughness critically determine the amount of elastic energy release and thereby the magnitude of earthquakes (Biegel et al., 1992; Harrington and Brodsky, 2009; Lay et al., 1982; Rubin et al., 1999). They characteristically produce linear surface roughness, formed by parallel long ridges and grooves structures, often called slickenlines, with their geometrical characteristics independent of the observation scale (Kirkpatrick and Brodsky, 2014; Sagy and Brodsky, 2009; Scholz and Aviles, 1986). The slip-surface roughness analysis is important not only to establish geologically past rupture events, but also to predict the boundary conditions of a possible future rupture episode in a region (Brodsky et al., 2016). Additionally, they are extensively used in paleo-stress calculations (Bott, 1959; Gudmundsson, 2011; Michael, 1984; Ramsay and Huber, 1987). Laboratory experiments suggest that the evolution of slip surface roughness can largely influence the frictional properties and in turn modulate the rupture propagation dynamics (Ohnaka and Shen, 1999; Okubo and Dieterich, 1984) and the frictional stability of a fault (Harbord et al., 2017; Marone and Cox, 1994; Ohnaka, 2013). Quantitative analysis of natural fault and shear surface roughness thus emerged as a challenging research front in brittle tectonics.

Early workers mostly used profilometer to measure the geometrical irregularities of fracture surfaces (Brown and Scholz, 1985; Lee and Bruhn, 1996; Power et al., 1988; Power and Tullis, 1991). The studies took a dramatic turn with the advent of non-contact type high-density optical scanning methods, leading to a remarkable improvement in the precision of field measurements (Bistacchi et al., 2011; Brodsky et al., 2011; Candela et al., 2012; Renard et al., 2006; Sagy et al., 2007). The quantitative analyses indicate a well-defined statistical characteristics of the surface features (Brown and Scholz, 1985; Candela et al., 2009; Lee and Bruhn, 1996; Power et al., 1987; Renard et al., 2006). Two major findings came out: 1) contrasting roughness along and across the slip direction (2-D profiles roughness along slip direction much smoother than that across the slip direction on particular length scales) (Renard et al., 2006), and 2) statistically self-affine, rather than self-similar properties. It has been demonstrated from analogue experiments that the degree of roughness anisotropy can progressively increase with increasing slip on shear surfaces. In addition, the experiments suggest a characteristic difference in one-dimensional fractal dimensions (ΔD) along and across the slip direction depending on the mode of shear failure and the initial fracture plane orientation (Mukhopadhyay et al., 2019). On the other hand, from 2D profiles several studies have reported self-affine fractal characteristics obeying a transformation $\delta x \rightarrow \mu \delta x, \delta z \rightarrow \mu^H \delta z$ (Candela et al., 2012), where δx is the profile length, δz is the asperity height and H is the roughness exponent, called the Hurst exponent ($H \neq 1$). It implies that the profile geometry of surface irregularities or asperities, e.g., sharpness varies with the scale of observations.

A number of slip events or a continuous stable sliding movement is accumulated to produce a finite displacement on a fault. However, detailed mapping of slip fields associated with an earthquake event, e.g., Imperial Valley earthquake shows a strongly non-linear distribution, where slips of large magnitudes localize in discrete domains, leaving some regions with little or no slip (Renard et al., 2013; Renard and Candela, 2017). Several co-seismic kinematic inversion models clearly suggest that slip events at the time of major earthquakes occur heterogeneously on the rupture surfaces. Such heterogeneous kinematic fields consist of isolated large-slip zones, called 'asperities', separated by no-slip regions, called 'barriers', as defined by a group of seismologists (Archuleta, 1984; Mai and Beroza, 2002; Renard and Candela, 2017). This kind of slip heterogeneity is thought to result from spatially non-uniform stress intensification along the fault surface, where the asperities locally builds high shear stresses to produce large slip at the moment of shear failure during an earthquake event (Candela et al., 2011a, 2011b). Heterogeneities in the stress fields can originate from various factors, such as roughness and compositional variations along the fault surface (Mai and Beroza, 2002) or can evolve as a consequence of the transient dynamics in the course of rupture propagation (Cochard and Madariaga, 1994). Causse et al. (2010) have shown self-similar fractal nature of the heterogenous distributions of asperities and barriers. It follows from the preceding discussion that fault kinematics is extremely complex due to an interplay of roughness and co-seismic slip and their strongly heterogeneous characteristics. Furthermore, this heterogeneity occurs on a wide range of spatial scales on the fault surface. Understanding of their complex behaviour is crucial to interpret the slip and slip velocity

* Corresponding author.
E-mail address: nibir.mandal@jadavpuruniversity.in (N. Mandal).

patterns on a fault in space and time (Candela et al., 2011a, 2011b; Manighetti et al., 2005). Although the earthquake-based studies have reported the slip heterogeneity phenomena, experimental investigations are required to validate them and explore how slip zones evolve during the fault movement. Our present article aims to meet this gap in the study of fault slip patterns.

We use linear roughness (slickenlines) of shear surfaces observed in the Singhbhum Shear Zone (SSZ) to study the geometrical patterns of slip zones in association with stick (non-slip) zones. This roughness mapping reveals intervening stick zones characterized by weakly developed linear features. We then performed analogue laboratory experiments to find the factors controlling the slip versus stick zone formation on shear surfaces. The experiments show a transition from stick to slip zone dominated kinematics as a function of the initial orientation of shear surfaces with respect to the compression direction. Using the difference between along- and across-slip 1D fractal dimensions as a quantitative parameter, we show contrasting roughness characteristics of the slip and stick zones from both field and experiments. Finally, this article provides a discussion on the implications of our experimental findings in interpreting slip-driven geological phenomena, such as earthquake localization.

2. Field studies

2.1. The Singhbhum Shear zone

The Singhhum Shear Zone (SSZ) is a ~200 km long, about 2 km wide arcuate ductile to brittle-ductile shear zone (Ghosh and Sengupta, 1987; Sengupta and Ghosh, 1997) in the eastern Precambrian terrain (Fig1a). The SSZ delineates the boundary between the North Singhbhum Mobile Belt (NSMB) of Proterozoic age in the north and the Archaean cratonic (Singhbhum Craton) nucleus to the south (Saha, 1994). It trends NW-SE in the eastern flank, turning to E-W in the central part and finally to NE-SW on the opposite flank, and always maintains northerly steep dips (40° to 60°). Structural studies suggest localization of large deformations over the entire stretch, however, with local variations in the intensity of ductile to brittle-ductile shearing (Roy et al., 2021; Sengupta and Ghosh, 1997).

We carried out our field studies in an elegant exposure of sheared quartzite at Patherogora village, located (22°32′37.911″N, 86°26′31.223″E, altitude: 143 m, accuracy: ±3 m) near the old Surda copper mines in the south-eastern flank of SSZ (Fig. 1a). The Patherogora-Surda area constitutes an undulating plateau, showing a spectacular range of scattered hills with an average altitude of about 200m. Geographically, the area lies between Mosabani in the east, Surda in the west, Dhobani ranges on the south and in the north, and can be accessed from the Mosabani- Tatanagar Road running parallel to the SSZ. In these scattered hills there are large outcrops of sheared quartzite, providing an excellent scope for studying slip-surface features on slickensides. We chose fresh shear surfaces with no significant weathering effects.

2.2. Approach

We selectively chose sheared quartzite outcrops displaying well-developed slickensides on a scale of a few centimetres to several meters, which allowed us to delineate slip zones by using linear features (slickenlines). Slickensides surfaces strike broadly parallel to the NW-SE trend of SSZ in its eastern flank, and the slickenlines on them plunge in the NE direction. Slip zones marked by strong linear features occur in discrete patches with intervening stick zones, which are either devoid of prominent slip parallel lineation or contain weakly developed lineation. Slip and stick zones were seen to coexist in several forms, such as random, irregular patches, alternate elongate bands, pits and grooves and circular slip zones, surrounded by lineation-free stick zones. Detailed photographs were taken to capture these patterns on varied scales to study the slip heterogeneity on shear surfaces. For a quantitative 3D analysis of shear surface roughness, we took their casts from selected locations (Figs 2a-d) and prepared their three-dimensional topography using a laser scan system in the laboratory.

2.3. Characteristics of shear surface roughness

Based on the surface roughness characteristics of slickensides, we demarcated the two principal domains: 1) slip zone and 2) stick zone (methods described in Supplementary). The main feature used to characterize them is the linear anisotropy in surface roughness, defined by ridge-groove 3D wave geometry in single or multiple orders of wavelengths. Slip zones characteristically show a strong linear anisotropy of roughness (discussed later). The roughness becomes almost isotropic in stick zones, represented by smooth or pitted or irregularities without any directional attribute.

Understanding the fault surface topography is an essential step to deal with the heterogeneous stress field that plays a critical role in the nucleation of isolated slip zones, triggering earthquakes (Campillo et al., 2001; Voisin, 2002), and propagation and arrest of the ruptures (Voisin et al., 2002). In our field studies, we thus meticulously observed how slip and stick zones are spatially correlated on slickenside surfaces. Their distributions are found to be neither uniform throughout the outcrop nor entirely random, rather they form specific geometrical patterns. The slip zones are often separated by linear stick zones parallel to the lineation (Fig. 1b). In places, the stick zones occur sporadically as discrete patches on the shear surface. These patches appear like islands surrounded by slip zones on all sides (Fig. 1c and d). Slip and struck zones also occur alternately to form a band structure almost parallel to the overall slip direction (Fig. 1e and f). Shear surfaces occasionally contain large slip zones surrounded on all sides by no-slip

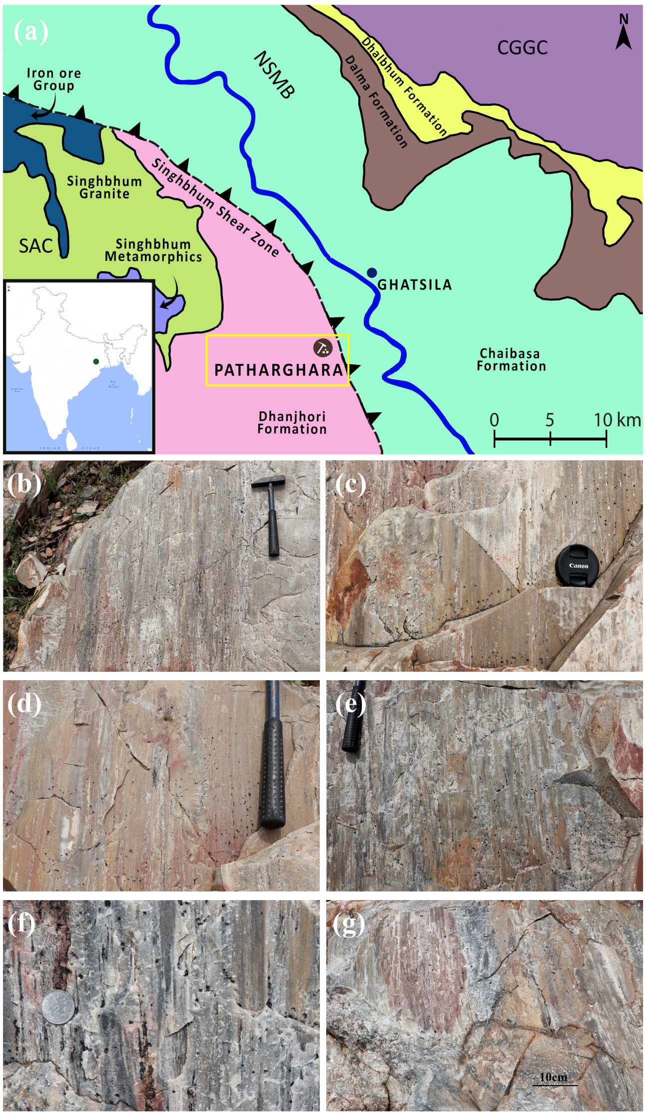

Fig. 1. (a) Geological framework of the Singhbhum Craton in the eastern part of India (location marked by green dot in the inset). The Singhbhum Shear Zone (SSZ) separates the Singhbhum Archean Craton (SAC) and the North Singhbhum Proterozoic mobile belt (NSMB) and Chhotonagpur Granite Gneissic Complex (CGGC). The yellow box demarcates the study area in the SSZ. (b) to (g): Field photographs of slickensides showing different geometrical relationships between slip zone (strongly lineated region) and stuck zones (regions with weak or no lineations). (b) Slip and stuck zones separated by a linear divisor. (c) and (d) Stuck zones surrounded by slip dominated zones on all sides. (e) and (f) Slip and stuck zones distributed all over the shear surface, forming a network. (g) Circular slip zones rimmed by an annular stuck region. (The hammer length= 33 cm, hammer handle length= 17.5 cm, camera cap diameter= 5.5cm, coin diameter= 2.5cm.)

domains in the form of an annular ring (Fig. 1g).

Several 1D analyses of natural fault-surface topology have indicated the roughness as a scale invariance phenomenon (Lee and Bruhn, 1996; Power et al., 1988, 1987; Power and Durham, 1997; Power and Tullis, 1991; Schmittbuhl et al., 1993). Such scale invariance characteristics can be described by self-affine geometry with a roughness scaling exponent. Our field observations reveal similar scale independent geometrical properties of slip and stick zones on slickensides. The different types of their geometrical patterns described above can be found on a wide range of spatial scales, from outcrop (tens of meters) (Fig. 1b) to hand specimen (a few centimetres) (Fig. 1e). Laser scanned images of the field casts (Fig. 2) further suggest that similar geometrical patterns of the slip and stick zones persist even in much smaller scales.

3. Laboratory Experiments

3.1. Method

We conducted analogue experiments on wet talc blocks, mixed with a small amount of white cement to introduce initial cohesion in the block. This wet talc material reproduced brittle-ductile rheology, and underwent shear failure at yield stress of 162 kPa, followed by a remarkable stress drop with increasing strain (Fig. 3a), i.e., strain softening after the first yield point (Brooks et al., 1991). The shear surfaces in talc models developed excellent one-dimensional irregularities, giving rise to typical slickensides features (Mukhopadhyay et al., 2019).

We used commercial talc powder (grain size: 0.3 to 50 μm, average: 20 μm) to prepare the analogue model in the following way. White cement and water were added to the pure talc powder in volume ratios, 1:6 and 1:9, respectively. The wet homogeneous mixture was then moulded in a rectangular box of desired dimensions [17.5 cm × 9 cm × 7.62 cm] to form a solid block. The purpose of using a little amount of white cement was also to retain the slip-induced geometrical irregularities produced shear surfaces after the experimental run and study them under the laser scanner system. The talc model was deformed in pure shear under a plane strain condition. The deformation setup is schematically illustrated in Figure 3b. In order to restrict the flow in the vertical direction, we fixed a horizontal toughened glass plate at the top model surface, allowing the model extension entirely in the horizontal direction, perpendicular to the horizontal shortening direction. This kinematic configuration sets a stress frame, defined by a vertical intermediate principal axis of stress (σ_2) and horizontal major and minor principal axes of stress (σ_1 and σ_3). To minimize friction at the basal and top model interfaces, we spread liquid soap (viscosity ~ 1.5 Pa s) at the model base and the bottom face of the top cover glass plate.

The talc model had an initial cut which reactivated to localize a shear surface during the experimental run. The purpose of introducing this cut was to simulate a shear surface at a desired inclination (θ) to the compression direction (σ_1-axis). It is noteworthy that the slip mechanism mediated by stick and slip zone formation is sensitive to θ. We implemented this approach in the following way. The talc block was cut into two halves at a desired orientation (θ). The two halves were then reunited, leaving the setup undisturbed for about ~2 hours and allowing the cut zone to heal sufficiently. The cut zone, however, remained as a weak planar heterogeneity, and facilitated the shear failure to localize in the talc model preferentially along its trend during pure shear deformation. We ran a series of experiments by systematically varying θ in the range 30° to 60°.

The convergence movement (6 mm/min) of two stepper motor driven pistons on opposite sides of the deformation table gave rise to a bulk shortening in the model at a rate of 2.2×10^{-3} s^{-1}. An experimental run was continuously monitored and photographed through the top glass plate, keeping the camera attached to an adjustable vertical stand, which was fixed to the deformation table. We used a computer-controlled automated shutter operation to capture successive snaps of the ongoing model deformation at regular intervals. Under compression, shear deformation localized along the vertical initial cut in the model to produce a laterally persistent shear surface. It was not possible to undertake in-situ observations of the shear

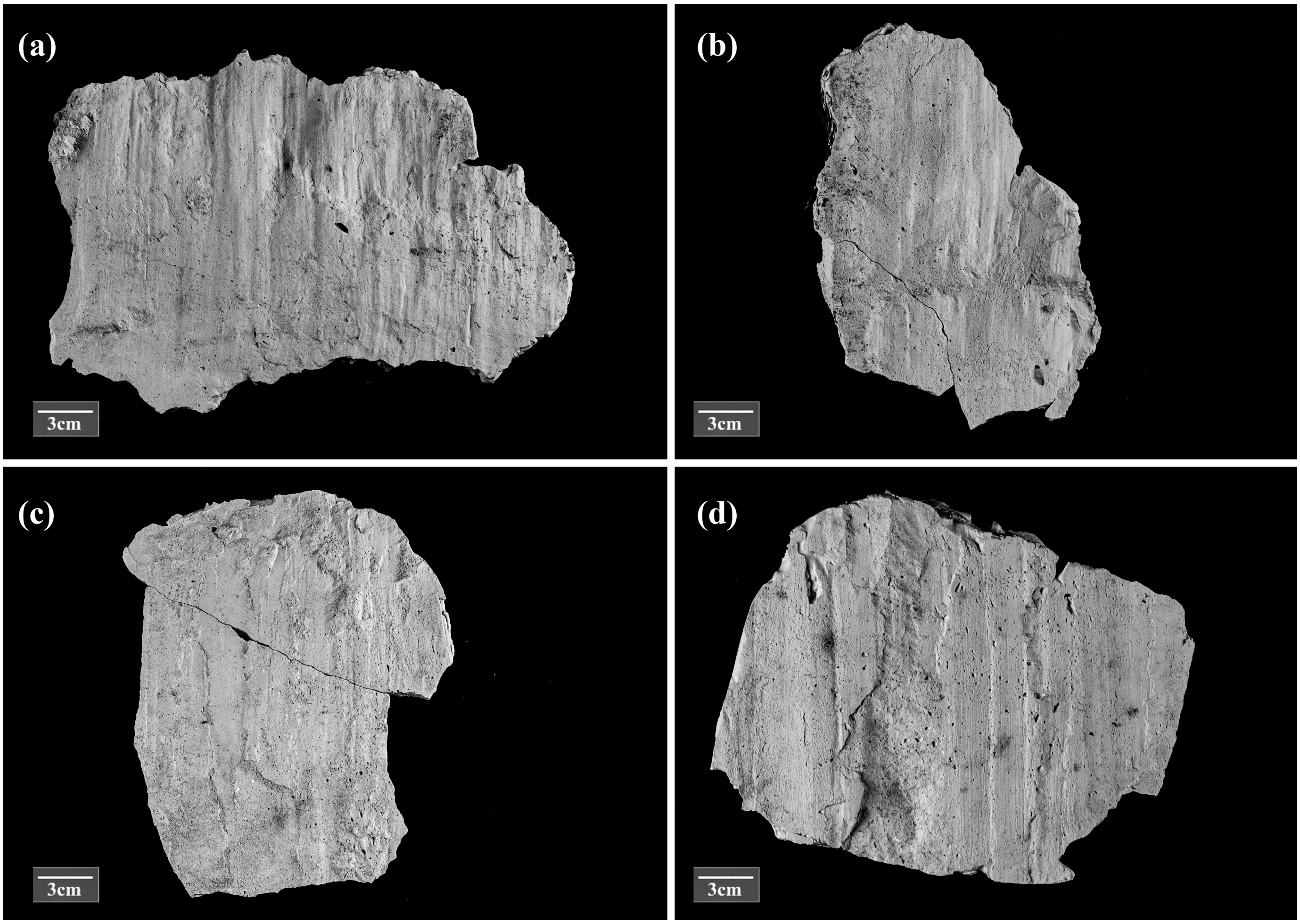

Fig. 2. Field casts of slickensides with various spatial slip-stuck zone patterns. (a) Shear surfaces containing linear roughness on wavelengths, ranging from a fraction of millimeter to a centimeter, and sporadic small non-lineated (stuck) regions. (b) Shear surface with wavy irregularities, as in (a), but showing more prominent stuck zones (> 45% in area coverage). (c) Slip-parallel lenticular stuck domains (> 53% in area coverage), often fingering inside the slip zones. d) Shear surface dominated by slip zones, leaving stuck zones as a minor component (20% in area coverage).

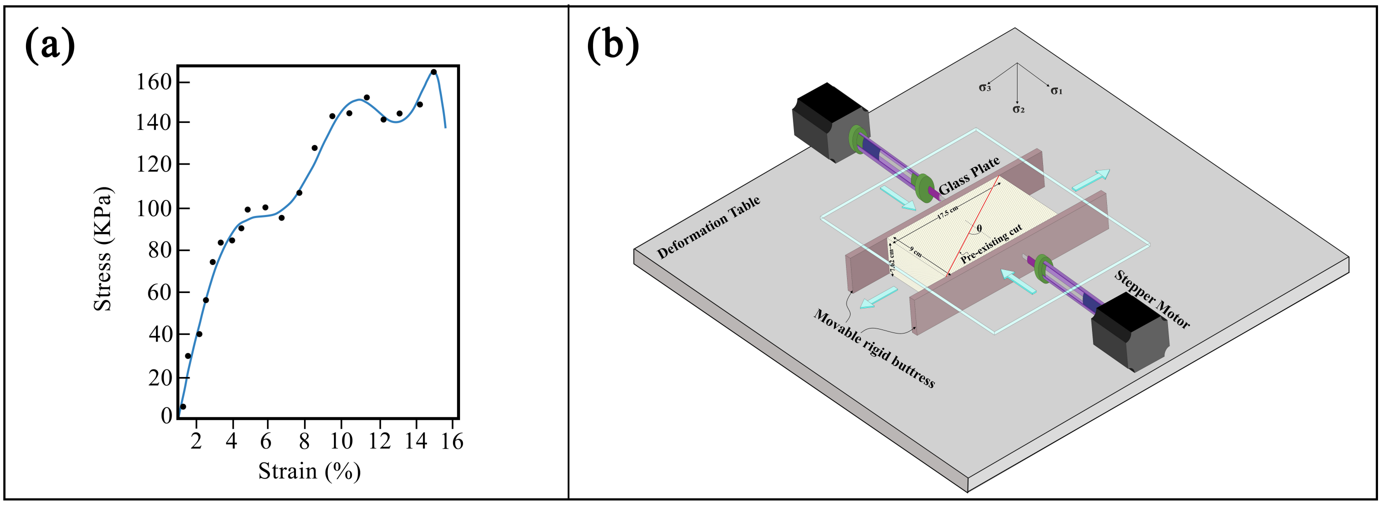

Fig. 3. (a) Stress versus strain plot from tri-axial creep tests to show the yield behavior of talc mixture (model material). The major failure occurred at 162 kPa. (b) Schematic of the laboratory setup for talc model experiments in pure shear (operational details given in the text).

surface topography during the experimental run. Earlier studies showed that shear surface features can significantly change with increasing finite slip (Brodsky et al., 2011). In our experiments, we thus kept model shortening low so that the finite slip remained roughly below 20% of the shear surface length. The deformed block was left untouched for about a day, allowing the block to harden and freeze the slickensides on the slip surfaces. The two halves were separated from each other with special care to preserve the geometrical features on the shear surface. The shear surface features were photographed to study the slip and stick zone patterns. For their quantitative geometrical analysis, the model slip surface was also scanned under Micro-Epsilon opto NCDT ILD1420-25 Laser Sensor. We finally performed a fractal analysis of the stick and slip domains. The details of the Laser and the Fractal Analysis will be discussed in *section 4*.

3.2. *Effects of shear surface inclination (θ)*

Sand-talc models localized slip preferentially along the pre-existing weak planes under pure shear, producing major shear fractures. Some secondary fractures locally branched from the principal shear surface. The shear surface roughness, defined by irregularities of ridge and groove structures, produce a lineation in the slip direction. The slickenside surface also developed some secondary features, like step-like reliefs oriented at high angles to the slickenlines, closely resembling the typical steps observed on natural fault surfaces (Doblas, 1998; Gay, 1970; Lin and Williams, 1992). Varying fracture inclination θ resulted in a spectacular transition of the roughness characteristics.

The experimental slickenside surfaces form two prominent domains: isolated slip zones and stick zones (Fig. 4), as observed in natural rock samples (Fig. 1b-g and 2). The slip zones occur sporadically, leaving isolated stick zones, which are devoid of any slip-induced lineation and show either positive or negative reliefs. Isolated stick zones show a wide variation in their normalized dimensions (equivalent circular diameter), ranging as low as 0.79 mm to 59.18 mm. The relative area of stick domains in the total shear surface reduces with increasing θ (Fig. 4a - c). For $\theta >$ 45°, the smaller size population of stick zones dominates in the system, and the shear surfaces develop mostly slip zones, characterized by strong slickenlines when θ = 60° (Fig. 4c). The stick zones become a minor component, covering less than 10% of the total shear surface area. Based on the stick-zone distributions, the shear surface roughness in our experiments can be grouped into the following three categories. a) Shear surfaces contain random discrete stick zones within a spatially vast slip zone. b) Shear surfaces consists of stick and slip zones in the form of alternate bands

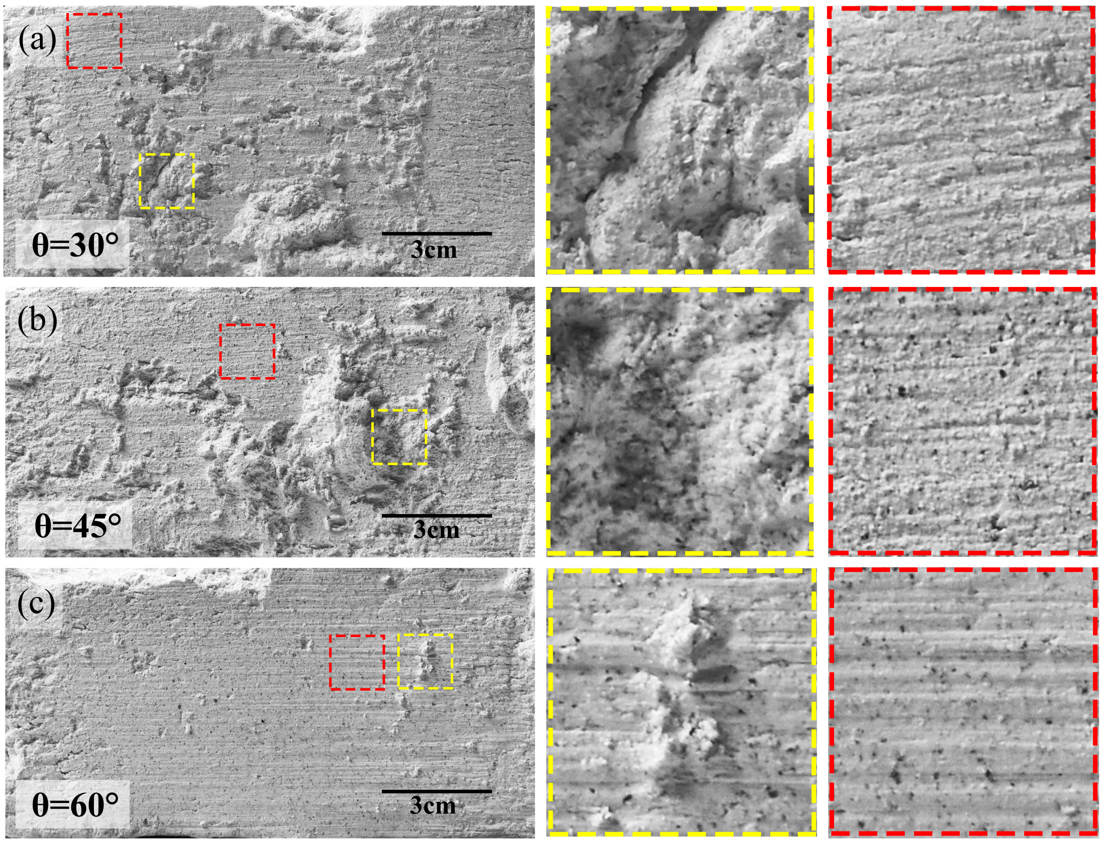

Fig. 4. Shear surface roughness produced in talc model experiments, conducted with varying initial shear-surface inclinations (θ) to the compression direction. The yellow and red boxes demarcate stuck and slip zones, respectively chosen for magnified views (corresponding right panels). (a) θ = 30°; shear surface with abundant stuck zones, characterized by roughness without any directionality. Notice intervening slip zones showing persistent slickenlines. (b) θ = 45°; nearly equal development of stuck and slip zones. (c) θ = 60°; extensive growth of slip zones, leaving small isolated stuck zones.

oriented parallel to the slip direction; c) Shear surfaces form a network of stick zones with slip domains.

4. Topological analysis of shear surface roughness

4.1. Objectives

We measured topographical fluctuations on shear surfaces to characterize their roughness properties (Renard and Candela, 2017), such as scale invariance and fractal dimension. The slickenline formation in slip zones results in surface irregularities with linearity, which is found to be a characteristic parameter of slickensides in fault zones (Mukhopadhyay et al., 2019; Renard and Candela, 2017). Several studies have shown that fault roughness can satisfy power-law size distributions of the geometrical irregularities (Candela et al., 2009; Mandelbrot et al., 1984; Power et al., 1987). Interestingly, the fractal dimensions (D) of such power-law distributions are often used to estimate the frictional properties of fracture surfaces; more the D values more the frictional strength (Hanaor et al., 2016; Popov and Filippov, 2010). In the present study, we undertake a laser-based roughness analysis to quantitatively describe the characteristic geometrical properties of the two shear-surface domains: slip and stick zones. This analysis uses the fractal dimension as a measure of roughness anisotropy in demarcating them.

4.2. Computational Methods

We used two methods: 1) MATLAB based image processing (Mukhopadhyay et al., 2019) and 2) laser profilometer to perform roughness analyses on outcrop and laboratory scales, respectively. In case of the image-based technique, surface illumination is the most crucial factor, where it must be sufficiently homogeneous over the surface area of interest. In a field environment, sunlight is the prime source of illumination, where its pattern varies during the day time due to a change of illuminating angle to the surface. To avoid this uncertainty, we chose a specific time of the day to capture images of slickenside surfaces of more or less uniform orientations (dip angle variation within ±3°). Special care was taken to set the DSLR camera in a fixed setting while capturing the images. The images were then processed in the MATLAB platform using the Gray Scale Intensity (GSI) values to prepare the topographic profiles of shear surfaces (Mukhopadhyay et al., 2019).

We developed a specially designed laser profilometer for the roughness analysis of experimental models and slickenside casts from the field. The setup consists of a rectangular bar frame, mounted with two parallel fixed rods and a motor-driven rotating spiral rod running in the middle of the parallel rods on one side of the frame (Fig. 5). The rotational motion of this rod produces a translational motion along its length direction (X-axis of the reference frame). The frame has a similar mechanical arrangement on its other side to produce simultaneously translational motion in Y direction (Fig. 5). The frame had two fixed draw-wire sensors to track the motion in X and Y directions. A point laser scanner is fixed to a plate at the end of a screw-driven holder, which allows us to move the sensor manually in the vertical direction (Z-axis) and set it at a desired height from the surface of the sample rested on the horizontal base of the frame. The height was adjusted to keep the scanning surface within the permissible range (25 to 50 mm) of the laser sensor. The rotational motion of the motor can be set at a desired speed (RPM range: 1 to 1000) and scan the sample surface at a specific horizontal velocity (range 10^{-5} m s^{-1} to 10^{-1} m s^{-1}) of the sensor in horizontal directions. We chose an optimum combination of the RPM and the sampling rate (500 s^{-1}) to obtain a desired resolution of the spatial data

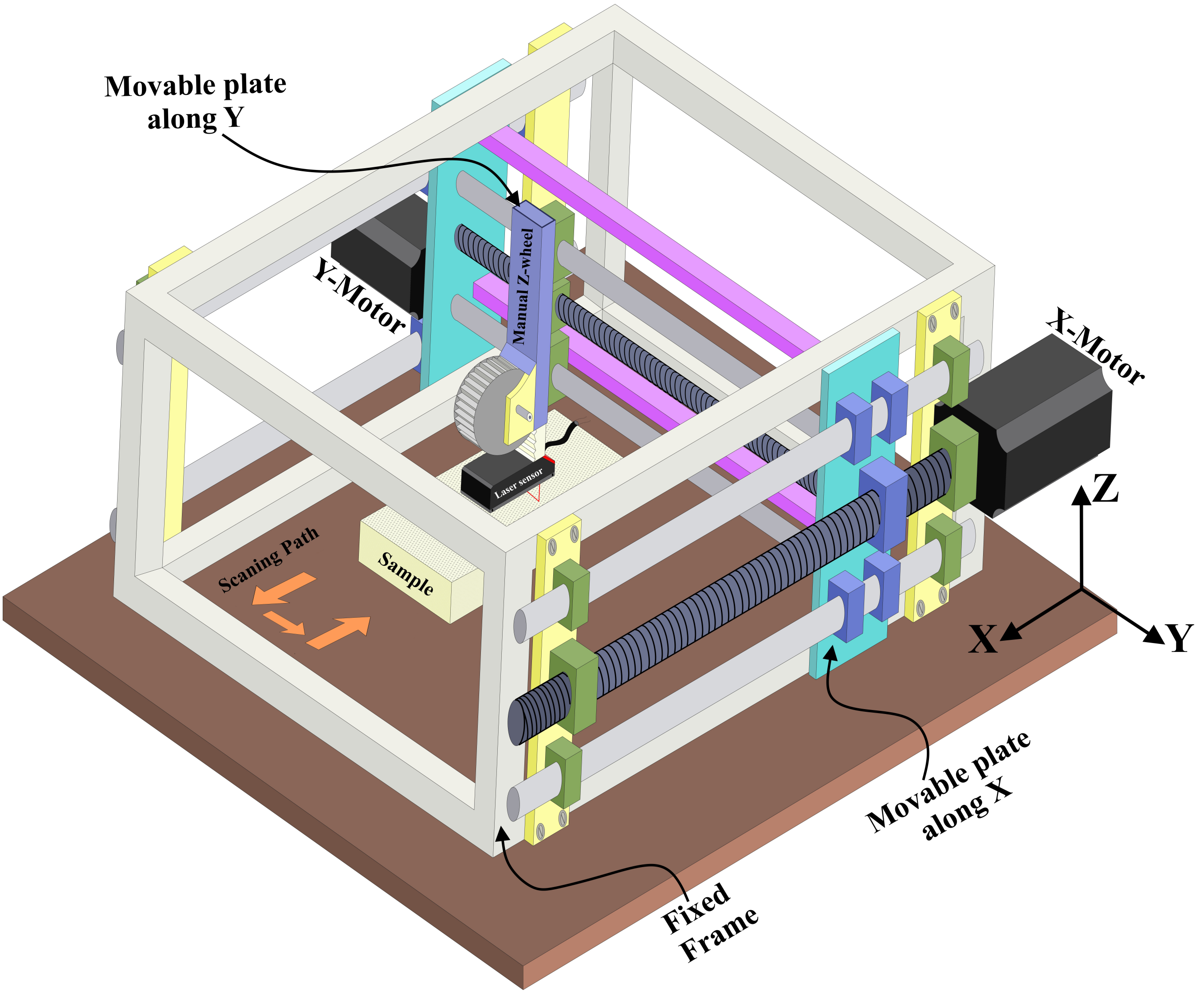

Fig. 5. A schematic presentation of the automated laser profilometer used for the 3D topographic analysis of shear surface roughness.

(60 μm). The laser scanning was performed by a to-and-fro motion of the sensor in horizontal directions, forward motion to cover X full length of scanning area → forward 1step in Y direction (0.06 mm) → backward X full length of scanning area→ forward 1 step in Y direction (0.06 mm). This sequence was repeated to cover the entire area of the sample surface. The electrical signals (voltage data) from the laser and the draw-wire position sensors were synchronously captured in a data acquisition system at the interface with a workstation. The acquired data were then processed using a software (3D Scanner by N K Instruments) code to the spatial distances, X, Y and Z. The data sets were then used to construct topographic profiles along and across the slickenlines, which were stacked to reconstruct a 3D topological surface with the help of MATLAB and CloudCompare software. We evaluated the areal occupancy of slip and stick zones on a shear surface using the ImageJ software.

4.3. Characterization of slip and stick zone roughness

4.3.1. Natural shear surfaces

As described in *section 2.3*, the exposed shear surfaces display linear roughness, formed by a preferred orientation of fine ridges and groves (slip zones), but they are locally devoid of any type of linearity in patches (stick zones). Figure 6 illustrates different varieties of roughness in natural shear surfaces, where the stick zones are delineated in transparent yellowish colour. A type of roughness contains distinct slip and stick zones; the latter occupies ~36 % of the shear surface area. A field example is presented to show two contrasting roughness domains, anisotropic slip zone and isotropic stick zone, with their boundary parallel to the slip direction (Fig. 6a). The corresponding profiles reveal a similar contrast between them in the GSI (Gray Scale Intensity) values, where the slip zones show higher amplitudes (GSI: ~50) than the stick zones (GSI: ~25). The profile of slip parallel and perpendicular direction of the stick zone shows a similar pattern (Difference in amplitude ~ 5 GSI values), implying an isotropic roughness characteristic. Another variety contains stick zones with patchy appearance. They are relatively rougher (GSI values: ~70) than the surrounding slip zones (GSI values: ~30) due to the presence of large-amplitude abundant ridges and grooves without any directionality. Along-slip profile of the slip zone is markedly smoother (GSI: 10-15) than an across-slip profile (Fig. 6b and c). Slickensides also show a network of stick zones with slip zones, broadly aligned in the slip direction. The corresponding across- and along-

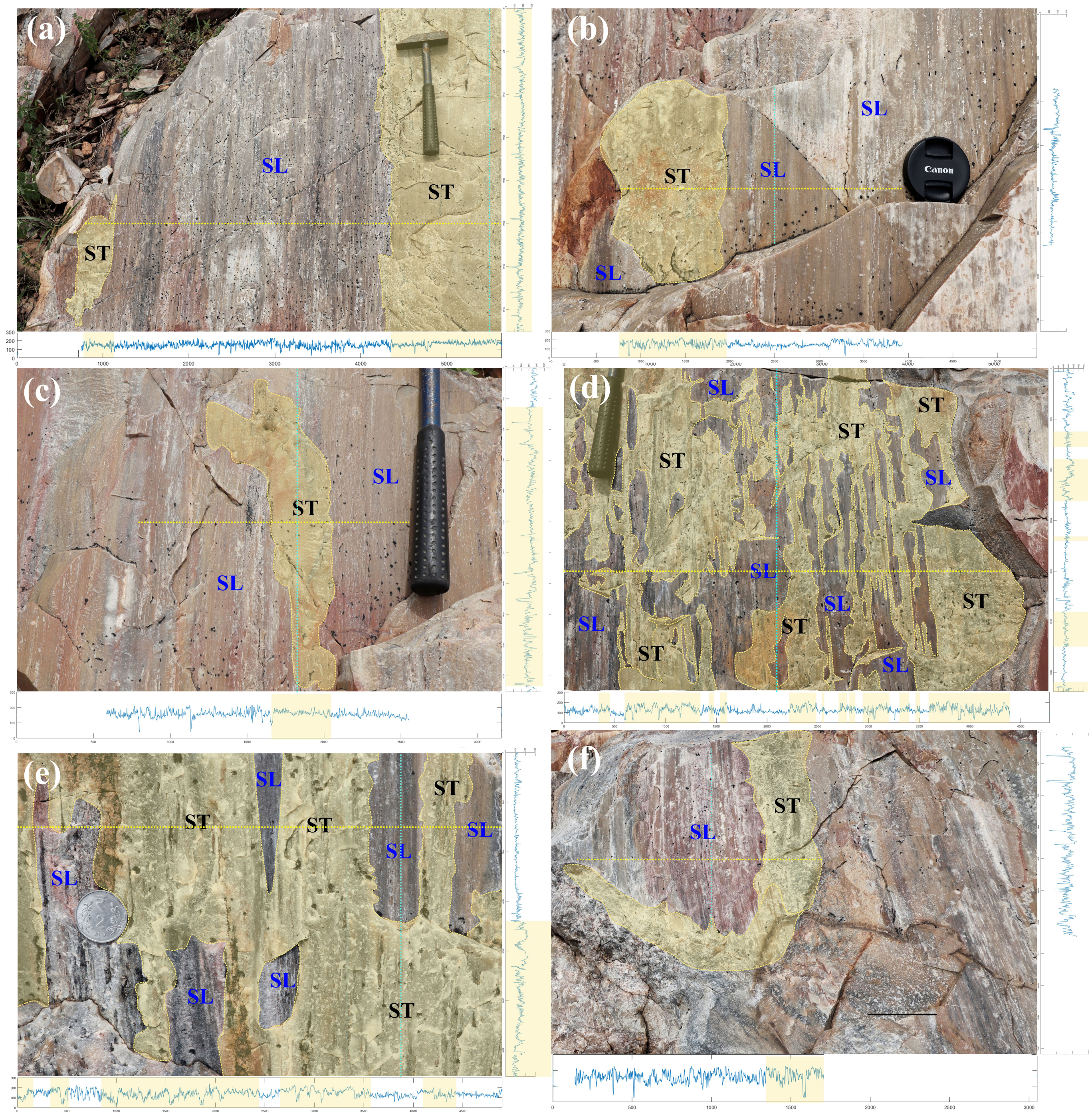

Fig. 6. (a-f) Field examples of varying roughness on shear surfaces in quartzite. Stuck zones (little or no lineation) are highlighted by light yellow shades. Corresponding across- (dotted yellow line) and along-slip (dotted cyan line) profiles are shown at the bottom and the right sides of each panel, respectively. ST: stuck zone, SL: slip zone.

slip profiles show a hybrid pattern of contrasting roughness, where the stick zones occur as bands of rougher irregularities in both the directions (GSI values ~ 60), which indicate their isotropic roughness property. In contrast, the slip zone profiles are characterized by a strong anisotropic roughness (across GSI: ~ 55 and along GSI: ~ 25) (Figure 6d and 6e). In places, slickensides display a unique roughness characteristics, where the slip zones occur in isolated patches, surrounded by stick zones (Fig. 6f). The slip zones show a large difference in the GSI values along and across the lineation.

The field casts were used for the roughness analysis in the laboratory with the help of the laser profilometer. We present a set of cast samples in Figure 7a-d, highlighting the stick zones in transparent grey colour to describe typical features of slip-stick zones association. A sample shows slip-dominated shear surfaces with minor stick zones (areal coverage: ~15 %) as isolated patches (Fig. 7a). The calculated 3D topography ensures the dominance of linear roughness, represented by a preferred orientation of alternate ridges and grooves, leaving small lineation-free domains (stick zones) (Fig. 8a). A magnified 3D view of the stick zones reveals isotropic roughness characteristics, giving rise to similar across- and along-slip profiles (amplitude ~ 1mm). In contrast, the slip zones consist of alternate linear ridges and grooves (see parallel colour bands in the topographic map) with a strong topographic anisotropy, which is evident from across- and along-slip profiles (slip perpendicular maximum amplitude ~ 3mm, whereas and slip parallel maximum amplitude ~1.5mm).

Figure 7b shows a field cast of shear surfaces characterized by competing slip and stick zones, which occupy 55 % and 45 % of the total shear surface area. The irregularities in lineated slip zones occur in two dominant wavelengths (~1 mm and ~ 10 mm), forming a multi-ordered topographic structure. The 3D topographic map also demarcates high lands, which are devoid of linearity (i.e. stick zones) and relatively flat regions of strong linearity (i.e., slip zones) (Fig. 8b). The domain-wise topographic mapping also allows us to distinguish between a stick zone and a slip zone in terms of their roughness characteristics. The directional topographic profiles of stick zones are almost identical (amplitude difference between across and along profiles ~ 0mm), but show a large variation in relatively smooth slip domains (amplitude difference ~ 1.9 mm).

Another example of field cast topography is presented in Figure 8c. The shear surface consists of stick zones as multiple bands, separated by slip zones. Their band structure is oriented broadly in the slip direction. The 3D maps show almost homogenous colour distribution, implying relatively a smaller variation of irregularity elevations (0.1 mm). The two domains: slip and stick zones, cover an area of 47% and 53% of the total surface area, respectively (Fig. 7c). The stick zone topography is characterized by uneven distribution of round pits and islands. Their corresponding profiles also show alternate but irregular valleys and peaks. In contrast, slip zones show fine scale slickenlines, giving rise to a remarkable difference in across- and along-slip topographic profiles. In extreme cases, slip zones far dominate (covering 80% of the total area) and stick zones localize in a few locations (Fig. 7d). The 3D topographical map shows a similar difference between the two domains (Fig. 8d), as described above.

4.3.2. Model shear surfaces

In laboratory experiments, shear surfaces produced stick zones mainly in the form of patchy domains. Their areal abundance varies inversely with the shear surface inclination (θ), reducing from ~ 56 % to 9% with $\theta = 30°$ to $60°$ (Fig. 9a-c). Their 3D topography, generated by laser profilometer shows a marked geometric difference between stick and slip zones, as observed in the field casts. Stuck zones form high or low lands without any directionality in their roughness, whereas slip zones in the model are relatively smooth, characterized by persistent linear roughness (Fig. 10a-c). The $\theta = 30°$ model shows topographically irregular domains (stick zones) spread over the shear surface, leaving relatively flat, isolated regions (slip zones) with linear topographic structures (ridge-groove) parallel to the slip direction (Fig. 10a(i)). Low-amplitude perturbations on the mean surface (5mm) of along-slip profiles clearly indicates smooth topography, as compared to that observed on an across-slip profile, which shows large amplitudes (8.5mm) of topographic roughness. This contrasting profile

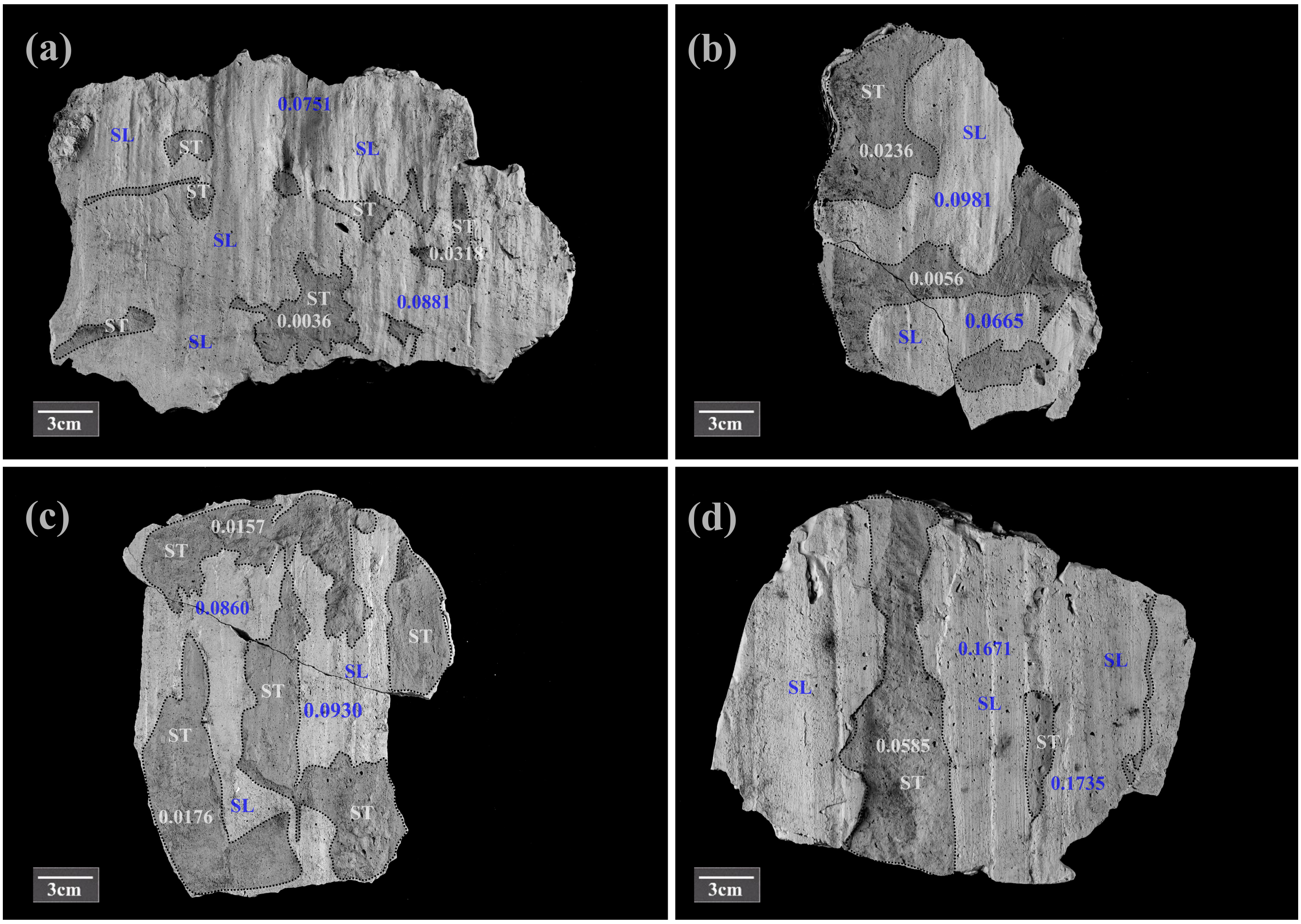

Fig. 7. (a-d) Stuck zone mapping (highlighted by grey shades) on shear surfaces from field casts. *ΔD* values are plotted in the stuck zones and slip zones (numbers in white and blue, respectively) to show a clear difference in their roughness anisotropy. ST: stuck zone, SL: slip zone.

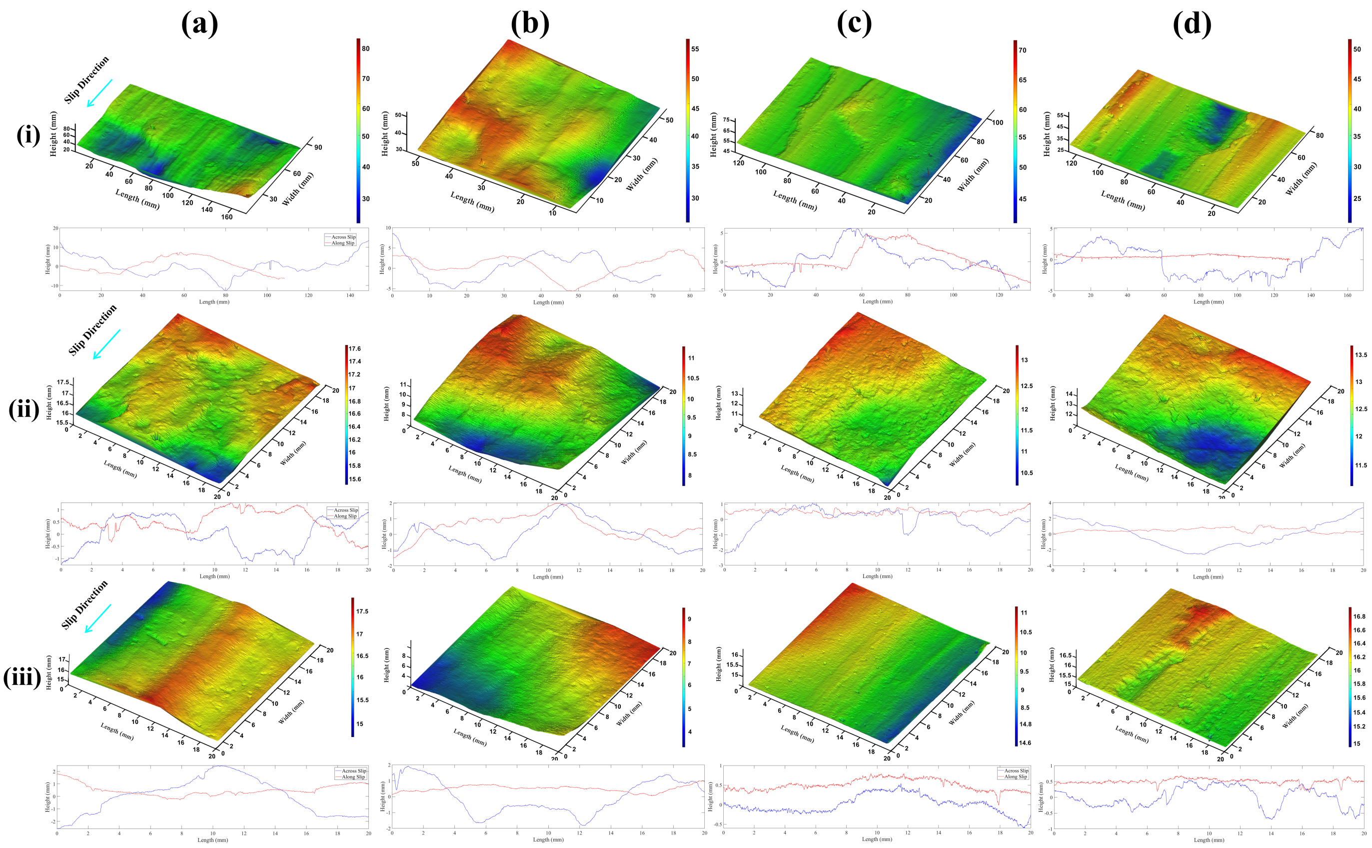

Fig. 8. (a) – (d) 3D topography of cast samples showing varying shear-surface roughness. Row-wise panels: (i) Surface topography containing stuck and slip zones; (ii) and (iii) Close views of stuck and slip zones, respectively. The corresponding across- and along-slip profiles are shown in red and blue lines at the bottom of each panel.

characteristics ensures the presence of linear roughness in slip zones, which is completely absent in stick zones, as revealed from similar along- and across-slip topographic profiles (Fig.10a(ii)). The slip zones, however, show strong heterogeneity in the degree of roughness anisotropy, especially weak in regions of irregular shear surface topography (Fig. 10a(iii)). The 3D shear surface topography produced for $\theta = 45°$ consists of two major topographic highs and a few small highs, along with numerous topographic low regions (Fig. 10b(i)). All these topographic elements represent stick zones with isotropic irregularities, which are broadly smoother (Fig. 10b(ii)) than those produced in the previous model ($\theta = 30°$) (Fig. 10a(ii)). The slip zones display coarse linearity, resulting in conspicuous roughness anisotropy in the 3D topology, which is also obvious from the difference in along- and across-slip roughness (Fig. 10b(iii)). The $\theta = 60°$ model produces slip zones to capture virtually the entire shear surface, leaving stick zones as a minor element (a few sporadic topographic highs and small pits) (Fig. 10c(i)). The enlarged views also reveal small islands of stick parts (Fig. 10c(ii)). The shear surfaces are remarkably smooth, but contain rod-like linear structures (dominantly in two wavelengths), forming a strong roughness anisotropy (Fig. 10c(iii)).

To summarize, increasing θ facilitates slip zones at the cost of stick zone areas, decreasing from 56% to 9%. The 3D stick zone topography develops increasing anisotropy with increasing θ (amplitude difference changes from 0.1mm to 0.7mm). An increase in θ intensifies the roughness anisotropy of shear surfaces.

5. Fractal analysis

We carried out a fractal analysis of shear surface roughness for both the field casts and laboratory models, aiming to find distinctive geometrical properties of the stick and slip zones. A fractal population of objects must obey a power law function: $N = C/r^D$, where N is the number of objects with linear dimension r, C is the proportionality constant and D is the fractal dimension (Turcotte, 1997). The number of objects, N will thus vary linearly with their corresponding size r in a *log-log* space. The principal two domains of a shear surface: stick and slip zones develop contrasting roughness anisotropy, as described in the earlier section. Using a box counting method we performed a one-dimensional fractal analysis to show the degree of anisotropy in terms of D.

We calculated D along and across the slip directions and considered their difference ΔD as a measure of roughness anisotropy. ΔD was evaluated independently for slip dominated and stick dominated zones in the field cast

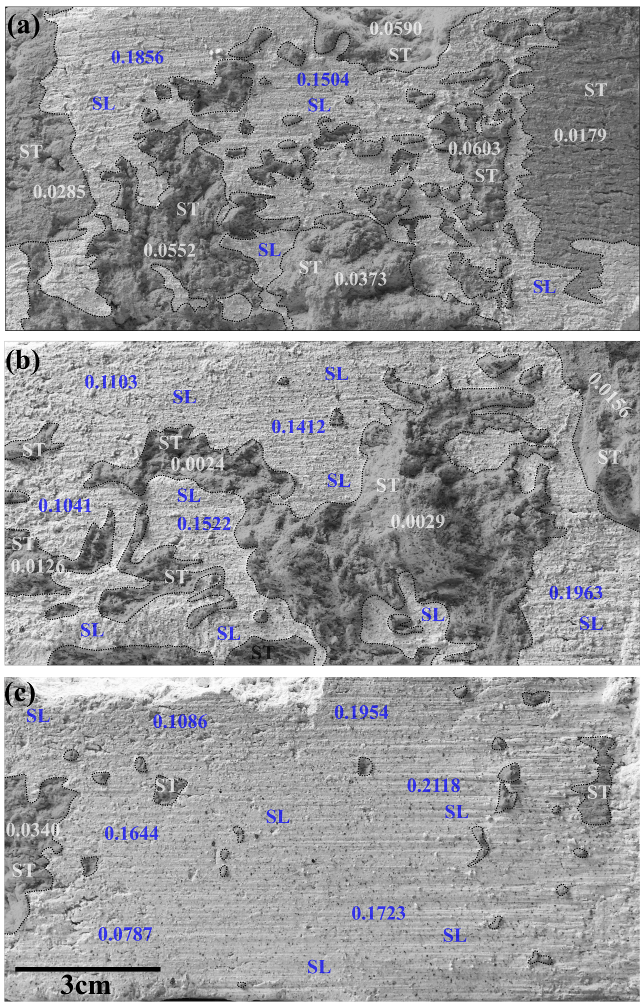

Fig. 9. Stuck zone mapping (highlighted by grey shades) of the shear surfaces produced in laboratory experiments. (a) $\theta = 30°$; (b) $\theta = 45°$ and (c) $\theta = 60°$. Numbers in white and blue color denote ΔD values of the stuck and slip zones, respectively. ST: stuck zone, SL: slip zone. It is noteworthy that stuck zones decrease in area, whereas slip zones increase ΔD with increasing θ.

samples as well as laboratory models. Our calculations yielded distinctive ΔD values in the two domains of shear surfaces (Figures 7 and 9). The stick zones in natural casts had ΔD (0.0036 to 0.0585) significantly lower than that in the corresponding slip zones (0.0665 to 0.1735). The contrasting ΔD is visually reflected in the difference of their roughness profiles along and across the slip direction (Fig. 8). Slip zones with strong slickenlines produce large ΔD values (~ 0.1735), implying quantitatively greater roughness anisotropy. On the other hand, low ΔD (= 0.0036) characterizes weak roughness anisotropy in stick zones, which agrees with the lack of directionality in their topographic irregularities. However, some of them had weak linearity, and gave rise to slightly higher ΔD values (ΔD = 0.0751 and 0.0881; Fig. 7a), albeit much lower than those obtained from slip zones with strong slickenlines (ΔD=0.1671 and 0.1735; Fig. 7d).

The fractal analysis of our analogue models produced ΔD values of shear surfaces strikingly in the similar ranges of ΔD for natural casts. The θ = 30° model yields ΔD in the range of 0.0179 to 0.0603 within stick zones, which is elevated to a range of 0.1504 to 0.1856 in slip zones (Fig. 9a). ΔD maintains a similar difference between the stick and slip zones in the θ = 45° model; stick zones: 0.0024 to 0.0156 and slip zones: 0.1041 to 0.1963 (Fig. 9b). As discussed earlier (*section 3.2*), stick zones were drastically reduced in area, from ~ 45% to ~ 9% of the shear surface when θ = 60° (Fig. 9c). Individual stick domains became so small in size it was hard to perform their roughness analysis using the box count method in a resolution required to find ΔD. Some of them occurred as islands of relatively larger size, which allowed us to calculate their ΔD (= 0.0340). Strongly lineated slip zones that covered most of the surface area (~ 91%) had large ΔD values in the range 0.0787 to 0.2118.

In summary, the slip domains of a shear surface are characterized by large ΔD values (> 0.07). Stuck domains, in contrast, form regions of low ΔD (< 0.06). Laboratory experiments suggest that increasing θ facilitates higher ΔD, implying an increase in the degree of roughness anisotropy of shear surfaces, as visualized from the difference between across- and along-slip profiles in their 3D topography (Fig. 10a(iii), b(iii), c(iii)).

6. Discussion

6.1. Roughness heterogeneity: its kinematic implications in earthquake mechanics

The kinematic inversion model of earthquake slip distributions predicted strongly heterogeneous slip fields from seismic faults (Fig. 11a), containing specific zones with the highest slip amplitudes, called asperity and zones with little or no slip, called barrier. The asperity-barrier combination geometrically resembles the slip and stick domains of our present concern. To test their genetic correlation, i.e., heterogeneous roughness characteristics as a manifestation of heterogeneous slip distribution, we performed an additional set of laboratory experiments, although it was designed for a low-resolution slip analysis (Detail method discussed in Supplementary S2). We used tracers on the pre-existing shear surfaces to track the slip amount during shearing. Some tracers had almost zero

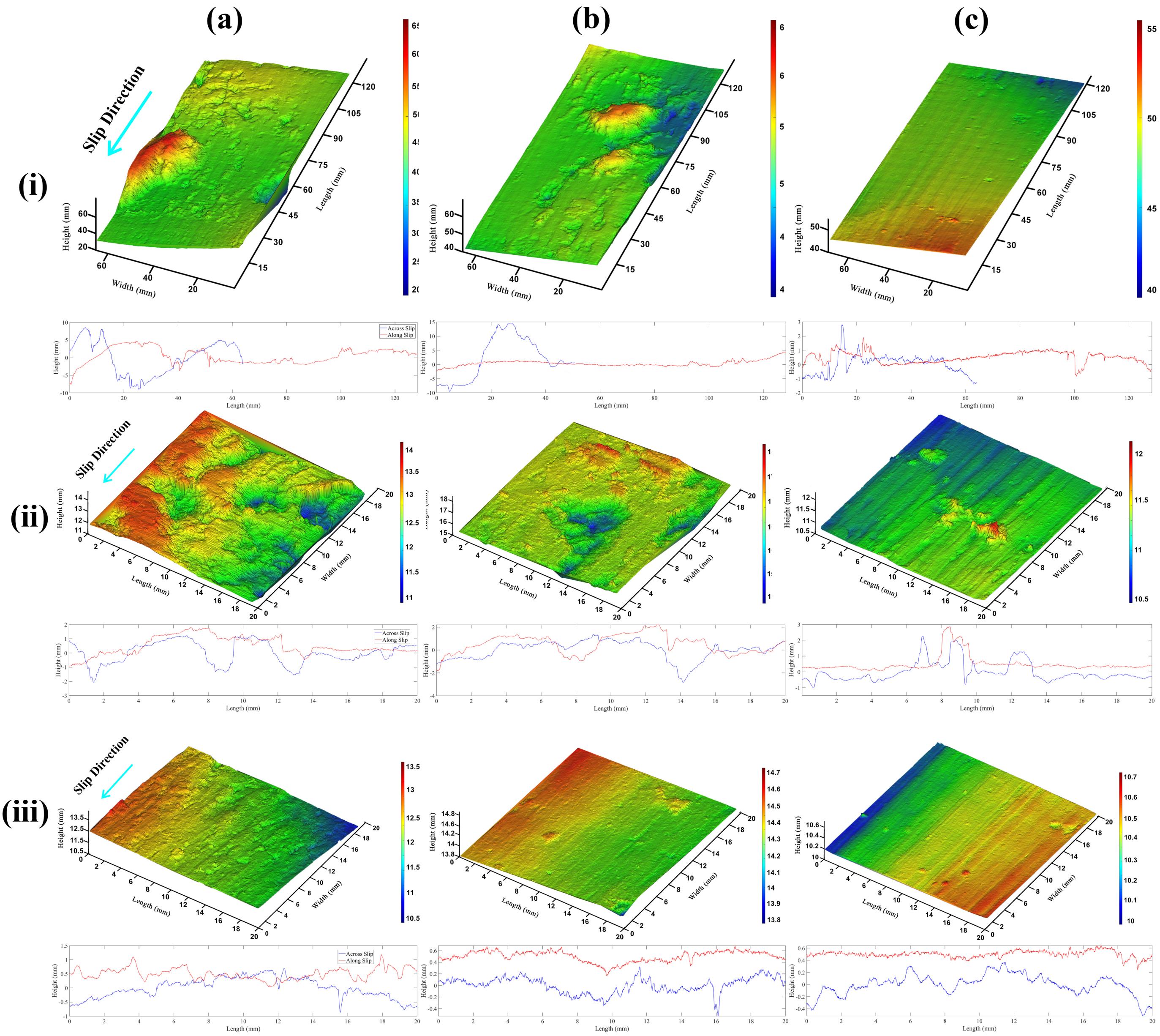

Fig. 10. Calculated 3D shear-surface topography in experimental models with θ = 30° (a), 45° (b) and 60° (c). Corresponding row-wise panels: (i) topography of the entire shear surfaces. (ii) and (iii) Selected portions of the shear surfaces to show the details of stuck and slip zone topography, respectively. Their across- (red lines) and along- (blue lines) slip profiles are placed below each panel.

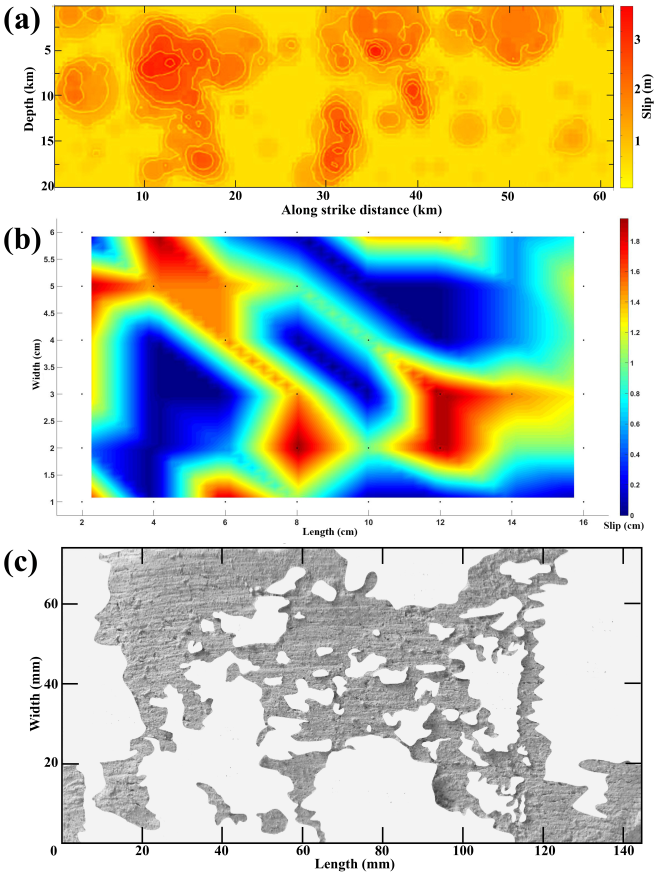

Fig. 11. (a) Spatial distribution of slip zones on a fault surface during the Kobe earthquake (modified after Zeng & Anderson, 2000). (b) Color map of heterogeneous slip fields on the fracture surface calculated from a slip analysis experiment (details provided in Supplementary S2). The colors represent slip amount in centimeter scale (refer to color bar). (c) Similar slip zone pattern in analogue experimental model with $\theta = 30°$.

movement (i.e., point of no slip), whereas some tracers showed a significant differential slip in the shear direction. The plot of their displacement vectors shows a heterogeneous slip distribution similar to that predicted from the slip inversion model (Fig. 11b and 11a). The asperity-barrier patterns geometrically match with the two roughness domains observed in the field as well as experiments (Fig. 6 and 11c). We thus assume that zones without any lineation are the manifestation of little or no slip regions, i.e., stick zone, whereas zones with prominent striations as the region of significant slip, i.e., slip zones. In the laboratory experiments the slip process on a shear surface operates randomly at all scales to produce a self-affine property of slip-stick (striated and non-striated) zone distributions, as reported from natural faults (Brodsky 2016).

Based on this experimental observation and the preliminary slip analysis models, we hypothesize that slip initiates randomly at isolated points on the shear surface, which independently grow in area to form a number of distinct zones with progressive bulk shearing. These slip zones continue to grow, and some of them break the stick zone barrier to coalesce with one another. However, some regions between two propagating slip zones are left unaffected by the rupture process and accommodate differential movement by ductile strains. These intact regions on the shear surface appear as zones characterized by no lineation or very feeble lineation. However, in course of deformation the slip domains can propagate through the stick zones and coalesce with the adjoining slip domains. The stick zone will then produce slickenlines in response to the onset of slip. In this slip-stick model, the slip domains are analogous to the asperities, the areas with the highest magnitude of slip on the rupture surface to generate earthquakes. The area around an asperity shows velocity strengthening (i.e., increase in sliding velocity give rise to higher frictional strength) (Collettini et al., 2019; Scholz and Campos, 2012), where the asperity shows velocity weakening (i.e., increase in sliding velocity lower the frictional strength) (Barbot, 2019; Dieterich, 1978). Ostapchuk et al., 2022 shows seismic patches, localized area of seismic source clusters corresponding to strong velocity weakening asperities, distributed over 50 ×15 km^2 areas that can sustain a 5 km long stick part in between.

Our analogue experiments show that the slip versus stick zone development at a given stage of shear surface evolution depends largely on the initial inclination (θ) of the shear surface to the principal compression direction. The stick zones virtually die out, as imprinted in negligibly small amounts of non-striated zones (~9%) for $\theta = 60°$). Using a mechanical model, we explain the positive impact of θ in facilitating the growth of slip zones and increasing roughness anisotropy at the cost of stick zones in the following way. Slickenlines observed in the experimental models had a matching morphology on either side of the shear surface. Previous studies have produced this unique type of slickenlines in a bi-viscous sandwich model (Mukhopadhyay et al., 2019) that demonstrates their origin in terms of "fold instability" in a thin low-viscosity layer (interface) between the strong walls. Increasing θ promotes this instability growth, which in turn facilitates the development of slickenlines and thereby enhances the roughness anisotropy (i.e., ΔD) on the shear surface (Fig. 9).

6.2. Geological and geophysical implications

Our study provides a new insight into the analysis of fault surface roughness that can be used to track heterogeneous slip kinematics and interpret a range of important fault-related geological phenomena, such as fluid permeability and earthquake locations. Roughness characteristics allows us to recognize two principal kinematic domains: stick zones (little or no slip) and slip zones (relative sliding motion). We discuss here, albeit in a qualitatively way to show how the ratio of slip to stick zone area (Ψ) would be a crucial parameter to determine these phenomena. Slip zone localization and their synkinematic growth enhance permeability in fault zones, which in turn facilitate fluid migration activities along the fault (Brown, 1987; Zimmerman and Bodvarsson, 1996). Our experiments suggest that Ψ increases steeply with increasing initial fault inclination (θ) to the compression direction (Fig.9). For example, $\Psi = 0.785$ at $\theta = 30°$, whereas $\Psi = 10.111$ when $\theta = 60°$. Faults oriented at high angles to the regional tectonic compression would be thus potential to develop area-wise extensive slip zones, and thereby act as preferential sites for more intense fluid activities. To summarize this discussion, this study recognizes slip to stick zone ratio as a possible factor for varying fault-driven fluid activities, as often encountered in many terrains (Faulkner et al., 2010).

The stick zone versus slip domains can also control the magnitude of strain accumulation on a fault surface. A stick zone acts as a locking agent to build elastic strains during fault movement partitioned in slip zones. Evidently, the amount of slip depends on the slip area, larger the slip zones larger the slip amount (Pollard and Segall, 1987). Small stick zones on fault surfaces are likely to fail to lock large slip movement and allow frictional displacements to dissipate mechanical energy, mediated by a number of secondary processes, such as frictional heating and secondary rupture formation. Stuck zones thus must form to cover a significant area of the shear surface so that they can act as an effective source for locking of the fault motion to develop large strains. On the other hand, the J integral analysis suggests that the amount of strain energy accumulated on a fault depends on the slip area (Atkinson, 1987). A large accumulation of strain energy required for high-magnitude earthquake generation demands slip zones on a large area. An optimum combination of slip and stick zones is thus a necessary condition to facilitate elastic strain accumulation and trigger earthquakes at the moment slip zones propagate by destabilizing their neighbouring stick zones (Atkinson, 1987). The spatial distribution of stick zones on the fault surface will eventually determine the temporal patterns of earthquake occurrence in a region. Our experiments suggest that stick and slip zones represent two competing processes, which would be controlled by the fault orientation with respect to the principal compression direction (θ). Stuck zones become extremely weak in their abundance when $\theta > 60°$. Faults with large θ would be thus less effective in the strain accumulation process, which play the most critical role in triggering earthquakes.

6.3. Fractal dimensions in the slip versus stick zone analysis

By combining field and experimental observations, we have recognized two geometrical domains of a fault surface, characterized by their distinctive surface roughness properties. Their detailed analyses provide a quantitative difference in roughness anisotropy, measured from along and across-slip profile amplitudes (Fig. 6, 8 and 10). We show that fractal dimension analysis can be an effective method to quantify the degree of roughness anisotropy. There are several other ways to measure contrasting roughness across and along slip profiles of irregular surfaces (Renard and Candela, 2017); one of them is Hurst exponent (H), where $H = 1.0$ indicates a self-similar roughness property (i.e., scale independent profile shapes), and $H < 1.0$ implies a self-affine roughness property (i.e., scale dependent profile shapes, becoming more and more smoother on increasing scale size). Renard and Candela (2017) performed a fractal analysis of synthetic 2D rough surfaces without any linear geometric elements and obtained equal H values in all directions. Their calculations yielded varying H with direction when the shear surfaces had slip induced lineation; H value (0.6) in along-slip direction was found to be less than H value (0.8) across-slip direction.

In this study, we have adopted a 1D fractal analysis taking into account the frequency of irregularity amplitudes to quantify the degree of roughness anisotropy. The difference between across- ($D_{\perp}$) and along-slip ($D_{\parallel}$) profile fractal dimensions ($\Delta D = D_{\perp} \sim D_{\parallel}$) is found to be significantly high (up to ΔD= 0.1735 in natural samples and 0.2118 in laboratory models) for slip zones, implying strong anisotropy in their roughness. Figure 12a shows a set of profiles at varying orientations to the slip direction. Their calculated fractal dimensions continuously increase from the parallel to perpendicular orientations ($D_{\parallel} = 0.8037$ to $D_{\perp} = 0.9513$; Fig. 12c). In contrast, stick zones show remarkably weak anisotropy, as reflected from little or no variation of D with the profile direction (ΔD = 0.0036 for casts and ΔD=0.0024 for laboratory models; Figs.12b and c). Based on the field observations and their experimental validation, we propose ΔD as an effective parameter in identifying slip and stick domains on a fault surface, as illustrated in Figure 12d. This can be a handy approach to calculate their relative abundance (stick to slip zone area ratio), which is a critical factor in controlling the pattern of earthquake events on a fault, as discussed in *section 6.1*.

6.4. Heterogeneous slip localization model

Frictional slip along well-defined shear surfaces and shear zones play a major role in the process of strain energy dissipation during crustal-scale tectonic deformations. As discussed in the preceding *section* (6.1), the morphological characteristics of shear surfaces can mediate the stress build-up and strain release cycles. Classical Coulomb-friction models account for uniform slip on a flat fault surface (Anderson, 1905; Angelier, 1979; Sibson, 2003). However, the slip behaviour during a seismic event as well as in the aseismic period is found to be extremely complex (Archuleta, 1984; Candela et al., 2011a, 2011b; Mai and Beroza, 2002; Rockwell and Klinger, 2013), hard to be predicted by such smooth-fault theory. It is now well-documented that faults always contains scale independent geometrical irregularities of the slip zones (Fig. 11a) (Zeng and Anderson, 2000), as observed in our present laboratory experiments (Fig 11c) and many earlier studies (Candela et al., 2011a, 2011b; Manighetti et al., 2005; Renard and Candela, 2017). The fault-slip fields are also strongly heterogeneous, both in terms of their magnitudes and directions. Theoretical studies demonstrated self-similar slip patterns (Hurst exponent of the spatial distribution, $H_S = 1$) (Andrews, 1980; Frankel, 1991; Herrero and Bernard, 1994). But, several field observations show self-affine characteristics of faults with H_S between 0 and 1 (Candela et al., 2011b). For example, Mai & Beroza, 2002 reported a self-affine analysis with average $H_S = 0.71 \pm 0.23$. The kinematic inversion models also suggest size dependence of the slip distributions and their governing factors (Causse et al., 2010). We performed a geometrical analysis of the irregular slip zones in our experimental models and obtained an excellent power law distribution, irrespective of θ value (Fig. 13). Their estimated 2D fractal dimensions, D = 1.7842, 1.9136 and 1.9793 for $\theta = 30°$, 45° and 60° respectively.

Our field observations at outcrop to hand specimen scales reveal variability in slickenlines characteristics, implying that the slip is not only heterogeneous, but also the shear surface is morphologically dissimilar in two principal domains: slip zones and stick zones. The laboratory experiments show their relative spatial occupancy varying with the shear surface orientation θ (Fig. 9). The stick zones are reduced in area, from 56% to 9% with an increase of θ from 30° to 60°, but their pattern continue to follow a power-law distribution (Fig. 13). Based on this experimental observation, we hypothesize that slip first localizes at isolated points on the

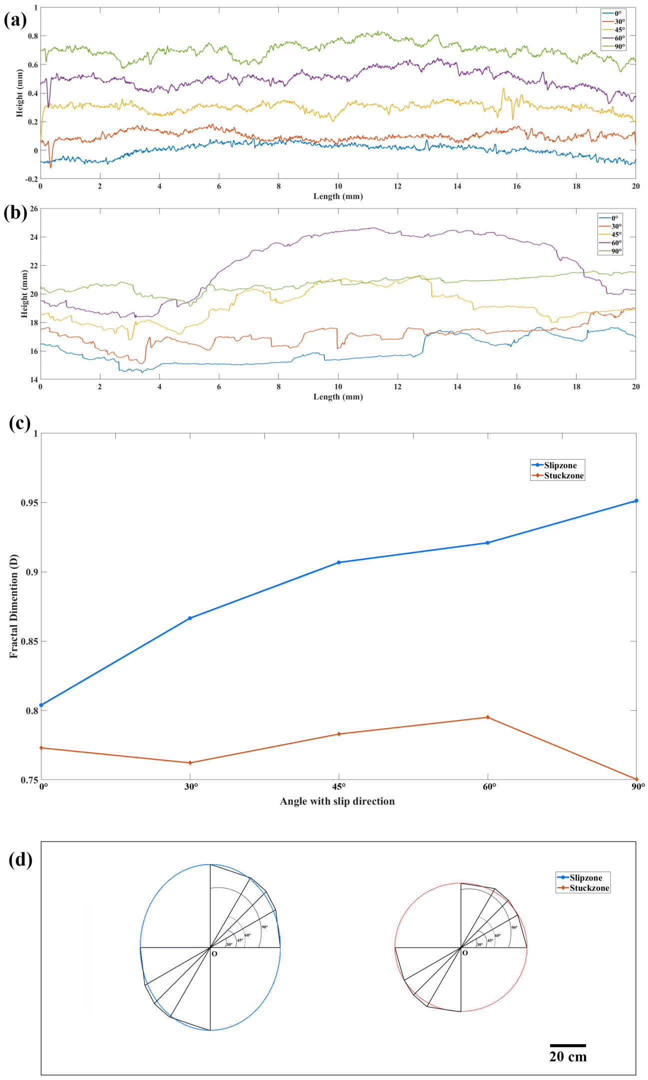

Fig. 12. (a) Variations of 2D roughness in slip zones with the profile orientation, 0° (parallel) to 90° (perpendicular) to the slip direction. Notice increasing roughness amplitude of the profiles from bottom to top. (b) Roughness profiles in a stuck zone for varying profile orientations. The profiles do not show any systematic roughness variation with the profile orientation. (c) Calculated plots of one-dimensional fractal dimension (*D*) of slip and stuck zone roughness as a function of the profile orientation. Notice a steady increase of *D* from parallel to perpendicular profile orientations in slip zones, but not in stuck zones. (d) Graphical presentations of the directional variability of *D* in slip and stuck zones. The radial length dimension represents the absolute value of *D*. The best-fit ellipse clearly reveals strong roughness anisotropy in slip zones, which becomes isotropic in stuck zones, as indicated by the circular graphical plot.

surface, which independently grow in area to form a number of distinct zones with progressive bulk shearing. These slip zones continue to grow, and some of them break the stick zone barrier to coalesce with one another. This sequential process takes place randomly at all scales to produce a self-affine property of slip-stick zone distributions.

Earlier theoretical and real slip data analysis as well as stress distribution models showed slip heterogeneity on the rupture surface of earthquake events (Candela et al., 2011b), as observed in our analogue model experiments. According to the pulse slip model, slip zones continue to propagate until they encounter a strong barrier (Brodsky and Mori, 2007). Stuck zones, characterized by isotropic surface roughness produced during a slip event can act as a barrier in the next sequence of slip events. Stuck zones can thus largely control the first order spatial patterns of coseismic slip localization during an earthquake event (Peyrat and Olsen, 2004). On the other hand, strong roughness anisotropy in slip zones, as shown from both field observations and analogue experiments, can contribute to directional stress accumulation on a fault surface (Marsan, 2006; Schmittbuhl et al., 2006).

6.5 Experimental limitations

The experimental method we have used in this study has a number of advantages. For example, the shear surface could be set at varied orientations to investigate how the slip versus stick zone processes can change with the initial shear surface orientations with respect to the

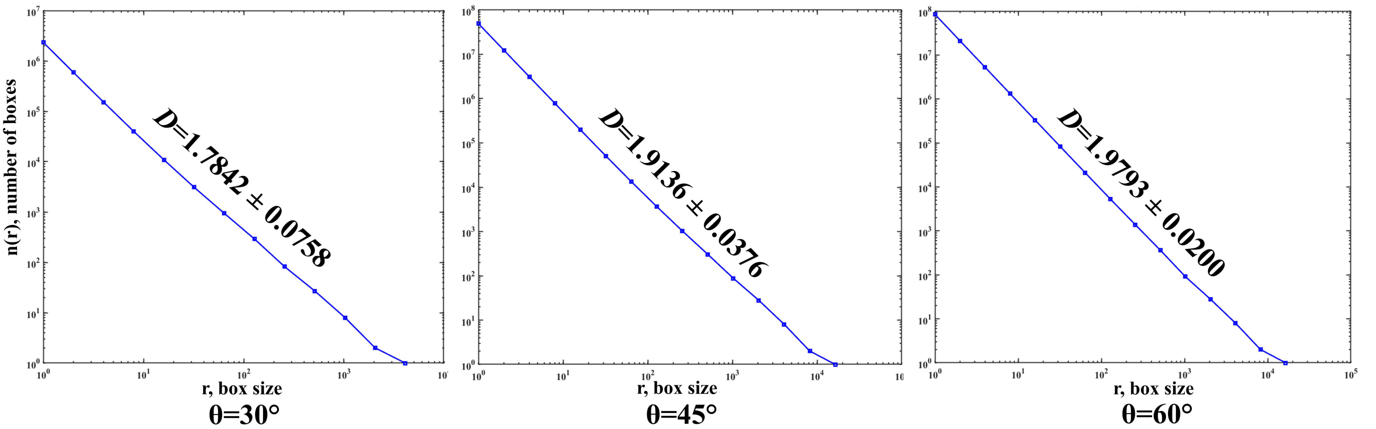

Fig. 13. Log-log plots of surface irregularities and their corresponding frequencies and the spatial fractal dimension, based on a 2D box-counting method. The linear plots indicate a power-law characteristic of the slip zones. Note that *D* increases with increasing *θ*.

compression direction. In addition, the experimental models allowed us to study the actual 3D topography produced on the shear surfaces using the laser profiling technique. Apart from these, the experimental method is cost-effective and can easily be implemented in a simple laboratory setup. However, there are a number of limitations, which are listed in the following. The experimental approach does not account for the role of frictional heating and associated phases changes, such as melting (Brown, 1998). These processes are reported to largely control the fault slip behaviour (Lee et al., 2017). Secondly, it was not possible to simulate other secondary processes like synkinematic mineral growth that often influences the shear surface roughness (Twiss and Moores, 1992). Finally, the effects of confining pressure and temperatures on the creep mechanisms that might operate during sliding movement along faults were excluded in our experiments.

7. Conclusions

We conclude the main outcomes of this study in the following points. 1) Intensely sheared quartzite in the Singhbhum shear zone extensively contains slickensides showing heterogeneous surface roughness, which allows us to recognize kinematically two distinct domains on the shear surfaces: stick zones and slip zones. Slip zones display strong anisotropy in their roughness due to the presence of linear structural elements (parallel ridges and grooves), whereas stick zones are devoid of any significant directionality in their roughness. 2) Four varieties of slip-stick zone associations are recognized in the field: i) slip and stick zones separated by a straight slip-parallel boundary; ii) sporadic stick zones occurring as islands with large slip zones; iii) band-like structures formed by alternate occurrence of stick and slip zones; iv) slip zones surrounded by stick zones. 3) The laboratory experiments suggest that the relative areal abundance of slip/stick zones on a shear surface is sensitive to the initial shear surface orientation (θ) with respect to principle compression direction. Increase in θ (from 30° to 60°) results in decreasing areal occupancy of the stick zones (56% to 9%). 4) The fractal analysis suggests that ΔD (difference in 1D fractal dimension across and along the slip direction) is an effective parameter to express the degree of anisotropy in surface roughness, and delineate stick and slip zones in field. ΔD attains its lowest value (0.0036) in stick zones, whereas the highest value (0.1735) in the slip zones. This field analysis is validated by the experimental data, where ΔD = 0.0024 (lowest value) and 0.2118 (highest value) in stick and slip zones, respectively. Increase of ΔD value with θ in experiments suggests enhancement of roughness anisotropy with strengthening of slip zones. 5) The amount of slip is strongly heterogeneous over the rupture surface for a single event due to the presence of stick zones. Slip zones can propagate by breaking the stick zones in course of slip events.

Acknowledgements

This work has been supported by the Science and Engineering Research Board (SERB), India through the J. C. Bose Fellowship (SR/S2/JCB-36/2012) to NM. UB and MM gratefully acknowledge the MoE, India and BRNS, India for the research fellowships awarded to them.

References

Anderson, E.M., 1905. The Dynamics of Faulting. Transactions of the Edinburgh Geological Society 8, 387–402. https://doi.org/10.1144/transed.8.3.387
Andrews, D.J., 1980. Fault impedance and earthquake energy in the Fourier transform domain. Bulletin of the Seismological Society of America 70, 1683–1698. https://doi.org/10.1785/BSSA0700051683
Angelier, J., 1979. Determination of the mean principal directions of stresses for a given fault population. Tectonophysics 56, T17–T26. https://doi.org/10.1016/0040-1951(79)90081-7
Archuleta, R.J., 1984. A faulting model for the 1979 Imperial Valley earthquake. Journal of Geophysical Research 89, 4559–4585. https://doi.org/10.1029/JB089iB06p04559
Barbot S. Slow-slip, slow earthquakes, period-two cycles, full and partial ruptures, and deterministic chaos in a single asperity fault. Tectonophysics. 2019;768. doi:10.1016/j.tecto.2019.228171
Atkinson, B.K., 1987. Introduction to fracture mechanics and its geophysical applications, in: Atkinson, B.K. (Ed.), Fracture Mechanics of Rock. Academic Press, pp. 1–26.
Biegel, R.L., Wang, W., Scholz, C.H., Boitnott, G.N., Yoshioka, N., 1992. Micromechanics of rock friction: 1. Effects of surface roughness on initial friction and slip hardening in Westerly granite. Journal of Geophysical Research 97, 8951–8964. https://doi.org/10.1029/92JB00042
Bistacchi, A., Griffith, W. A., Smith, S.A.F., di Toro, G., Jones, R., Nielsen, S., 2011. Fault roughness at seismogenic depths from LIDAR and photogrammetric analysis. Pure and Applied Geophysics 168, 2345–2363. https://doi.org 10.1007/s00024-011-0301-7
Bott, M.H.P., 1959. The mechanics of oblique slip faulting. Geological Magazine 96, 109–117. https://doi.org/10.1017/S0016756800059987
Brodsky EE, Kirkpatrick JD, Candela T. Constraints from fault roughness on the scale-dependent strength of rocks. Geology. 2016;44(1):19-22. doi:10.1130/G37206.1
Brodsky, E.E., Gilchrist, J.J., Sagy, A., Collettini, C., 2011. Faults smooth gradually as a function of slip. Earth and Planetary Science Letters 302, 185–193. https://doi.org/10.1016/j.epsl.2010.12.010
Brodsky, E.E., Mori, J., 2007. Creep events slip less than ordinary earthquakes. Geophysical Research Letters 34. https://doi.org/10.1029/2007GL030917
Brooks, N.W., Duckett, R.A., Ward, I.M., 1991. Investigation into double yield points in polyethylene. Polymer 33, 1872–1880. https://doi.org/10.1016/0032-3861(92)90486-G
Brown, S.R., 1998. Frictional heating on faults: stable sliding versus stick-slip. Journal of Geophysical Research: Solid Earth 103, 7413–7420. https://doi.org/10.1029/98jb00200
Brown, S.R., 1987. Fluid flow through rock joints: the effect of surface roughness. Journal of Geophysical Research 92, 1337–1347. https://doi.org/10.1029/JB092iB02p01337
Brown, S.R., Scholz, C.H., 1985. Broad bandwidth study of the topography of natural rock surfaces. Journal of Geophysical Research 90. https://doi.org/10.1029/jb090ib14p12575
Campillo, M., Favreau, P., Ionescu, I.R., Voisin, C., 2001. On the effective friction law of a heterogeneous fault. Journal of Geophysical Research: Solid Earth 106, 16307–16322. https://doi.org/10.1029/2000jb900467
Candela, T., Renard, F., Bouchon, M., Brouste, A., Marsan, D., Schmittbuhl, J., Voisin, C., 2009. Characterization of fault roughness at various scales: Implications of three-dimensional high resolution topography measurements. Pure and Applied Geophysics 166, 1817–1851. https://doi.org/10.1007/s00024-009-0521-2
Candela, T., Renard, F., Bouchon, M., Schmittbuhl, J., Brodsky, E.E., 2011b. Stress drop during earthquakes: Effect of fault roughness scaling. Bulletin of the Seismological Society of America 101, 2369–2387. https://doi.org 10.1785/0120100298
Candela, T., Renard, F., Klinger, Y., Mair, K., Schmittbuhl, J., Brodsky, E.E., 2012. Roughness of fault surfaces over nine decades of length scales. Journal of Geophysical Research: Solid Earth 117. https://doi.org/10.1029/2011JB009041
Candela, T., Renard, F., Schmittbuhl, J., Bouchon, M., Brodsky, E.E., 2011a. Fault slip distribution and fault roughness. Geophysical Journal International 187, 959–968. https://doi.org/10.1111/j.1365-246X.2011.05189.x
Causse, M., Cotton, F., Mai, P.M., 2010. Constraining the roughness degree of slip heterogeneity. Journal of Geophysical Research: Solid Earth 115. https://doi.org/10.1029/2009JB006747
Chester, F.M., Chester, J.S., Kirschner, D.L., Schulz, S.E., Evans, J.P., 2004. Structure of Large-Displacement, Strike-Slip Fault Zones in the Brittle Continental Crust, in: Rheology and Deformation of the Lithosphere at Continental Margins. pp. 223–260. https://doi.org/10.7312/karn12738-009
Cochard, A., Madariaga, R., 1994. Dynamic faulting under rate-dependent friction. Pure and Applied Geophysics 142, 419–445. https://doi.org/https://doi.org/10.1007/BF00876049
Collettini C, Tesei T, Scuderi MM, Carpenter BM, Viti C. Beyond Byerlee friction, weak faults and implications for slip behavior. Earth Planet Sci Lett. 2019;519. doi:10.1016/j.epsl.2019.05.011
Cowan, D.S., Cladouhos, T.T., Morgan, J.K., 2003. Structural geology and kinematic history of rocks formed along low-
Doblas, M., 1998. Slickenside kinematic indicators. Tectonophysics 295, 187–197. https://doi.org/10.1016/S0040-1951(98)00120-6
Dieterich JH. Time-dependent friction and the mechanics of stick-slip. Pure and Applied Geophysics PAGEOPH. 1978;116(4-5). doi:10.1007/BF00876539
angle normal faults, Death Valley, California. GSA Bulletin 1230–1248. https://doi.org/10.1130/B25245.1
Faulkner, D.R., Jackson, C.A.L., Lunn, R.J., Schlische, R.W., Shipton, Z.K., Wibberley, C.A.J., Withjack, M.O., 2010. A review of recent developments concerning the structure, mechanics and fluid flow properties of fault zones. Journal of Structural Geology. https://doi.org/10.1016/j.jsg.2010.06.009
Frankel, A., 1991. High-frequency spectral falloff of earthquakes, fractal dimension of complex rupture, b value, and the scaling of strength on faults. Journal of Geophysical Research 96, 6291–6302. https://doi.org/10.1029/91JB00237
Gay, N.C., 1970. The formation of step structures on slickensided shear surfaces. The Journal of Geology 78, 523–532.
Ghosh, S.K., Sengupta, S., 1987. Progressive development of structures in a ductile shear zone. Journal of Structural Geology 9, 277–287. https://doi.org/10.1016/0191-8141(87)90052-6
Gudmundsson, A., 2011. Rock fractures in geological processes. Cambridge University Press.
Hanaor, D.A.H., Gan, Y., Einav, I., 2016. Static friction at fractal interfaces. Tribology International 93, 229–238. https://doi.org/10.1016/j.triboint.2015.09.016
Harbord, C.W.A., Nielsen, S.B., de Paola, N., Holdsworth, R.E., 2017. Earthquake nucleation on rough faults. Geology 45, 931–934. https://doi.org/10.1130/G39181.1
Harrington, R.M., Brodsky, E.E., 2009. Source duration scales with magnitude differently for earthquakes on the San Andreas fault and on secondary faults in Parkfield, California. Bulletin of the Seismological Society of America 99, 2323–2334. https://doi.org/10.1785/0120080216
Herrero, A., Bernard, P., 1994. A kinematic self-similar rupture process for earthquakes. Bulletin of the Seismological Society of America 84, 1216–1228. https://doi.org/10.1785/BSSA0840041216
Kirkpatrick, J.D., Brodsky, E.E., 2014. Slickenline orientations as a record of fault rock rheology. Earth and Planetary Science Letters 408, 24–34. https://doi.org/10.1016/j.epsl.2014.09.040
Lay, T., Kanamori, H., Ruff, L., 1982. The asperity model and the nature of large subduction zone earthquakes. Earthquake Prediction Research 1, 3–71.
Lee, J.J., Bruhn, R.L., 1996. Structural anisotropy of normal fault surfaces. Journal of Structural Geology 18, 1043–1058. https://doi.org/10.1016/0191-8141(96)00022-3
Lee, S.K., Han, R., Kim, E.J., Jeong, G.Y., Khim, H., Hirose, T., 2017. Quasi-equilibrium melting of quartzite upon extreme friction. Nature Geoscience 10, 436–441. https://doi.org/10.1038/ngeo2951
Lin, S., Williams, P.F., 1992. The origin of ridge-in-groove slickenside striae and associated steps in an S-C mylonite. Journal of Structural Geology 14, 315–321. https://doi.org/10.1016/0191-8141(92)90089-F

Mai, P.M., Beroza, G.C., 2002. A spatial random field model to characterize complexity in earthquake slip. Journal of Geophysical Research: Solid Earth 107, ESE 10-1-ESE 10-21. https://doi.org/10.1029/2001jb000588
Mandelbrot, B.B., Passoja, D.E., Paullay, A.J., 1984. Fractal character of fracture surfaces of metals. Nature 308, 721–722. https://doi.org/https://doi.org/10.1038/308721a0
Manighetti, I., Campillo, M., Sammis, C., Mai, P.M., King, G., 2005. Evidence for self-similar, triangular slip distributions on earthquakes: Implications for earthquake and fault mechanics. Journal of Geophysical Research: Solid Earth. https://doi.org/10.1029/2004JB003174
Marone, C., Cox, S.J.D., 1994. Scaling of rock friction constitutive parameters: The effects of surface roughness and cumulative offset on friction of gabbro. Pure and Applied Geophysics 143, 359–385. https://doi.org/10.1007/BF00874335
Marsan, D., 2006. Can coseismic stress variability suppress seismicity shadows? Insights from a rate-and-state friction model. Journal of Geophysical Research: Solid Earth 111. https://doi.org/10.1029/2005JB004060
Michael, A.J., 1984. Determination of stress from slip data: faults and folds. Journal of Geophysical Research: Solid Earth 89, 11517–11526. https://doi.org/10.1029/JB089iB13p11517
Mukhopadhyay, M., Biswas, U., Mandal, N., Misra, S., 2019. On the development of shear surface roughness. Journal of Geophysical Research: Solid Earth 124, 1273–1293. https://doi.org/10.1029/2018JB016677
Ohnaka, M., 2013. The physics of rock failure and earthquakes, The Physics of Rock Failure and Earthquakes. Cambridge University Press. https://doi.org/10.1017/CBO9781139342865
Ohnaka, M., Shen, L., 1999. Scaling of the shear rupture process from nucleation to dynamic propagation: Implications of geometric irregularity of the rupturing surfaces. Journal of Geophysical Research: Solid Earth 104, 817–844. https://doi.org/10.1029/1998jb900007
Okubo, P.G., Dieterich, J.H., 1984. Effects of physical fault properties on frictional instabilities produced on simulated faults. Journal of Geophysical Research 89, 5817–5827. https://doi.org/10.1029/JB089iB07p05817
Ostapchuk A, Polyatykin V, Popov M, Kocharyan G. Seismogenic Patches in a Tectonic Fault Interface. Front Earth Sci (Lausanne). 2022;10. doi:10.3389/feart.2022.904814
Peyrat, S., Olsen, K.B., 2004. Nonlinear dynamic rupture inversion of the 2000 Western Tottori, Japan, earthquake. Geophysical Research Letters 31. https://doi.org/10.1029/2003gl019058
Pollard, D.D., Segall, P., 1987. Theoretical displacements and stresses near fractures in rock: with applications to faults, joints, veins, dikes, and solution surfaces, in: Atkinson, B.K. (Ed.), Fracture Mechanics of Rocks. Academic Press, pp. 277–349.
Popov, V.L., Filippov, A.É., 2010. Force of friction between fractal rough surface and elastomer. Technical Physics Letters 36, 525–527. https://doi.org/10.1134/S1063785010060118
Power, W.L., Durham, W.B., 1997. Topography of natural and artificial fractures in granitic rocks: Implications for studies of rock friction and fluid migration. International Journal of Rock Mechanics and Mining Sciences 34, 979–989. https://doi.org/10.1016/S1365-1609(97)80007-X
Power, W.L., Tullis, T.E., 1991. Euclidean and fractal models for the description of rock surface roughness. Journal of Geophysical Research 96, 415–424. https://doi.org/10.1029/90JB02107
Power, W.L., Tullis, T.E., Brown, S.R., Boitnott, G.N., Scholz, C.H., 1987. Roughness of natural fault surfaces. Geophysical Research Letters 14, 29–32. https://doi.org/10.1029/GL014i001p00029
Power, W.L., Tullis, T.E., Weeks, J.D., 1988. Roughness and wear during brittle faulting. Journal of Geophysical Research 93. https://doi.org/10.1029/jb093ib12p15268
Ramsay, J.G., Huber, M.I., 1987. The Techniques of Modern Structural Geology, Volume 2_ Folds and Fractures. Academic Press, London.
Renard, F., Candela, T., 2017. Scaling of fault roughness and implications for earthquake mechanics, in: Fault Zone Dynamic Processes: Evolution of Fault Properties during Seismic Rupture. pp. 197–216. https://doi.org/10.1002/9781119156895.ch10
Renard, F., Candela, T., Bouchaud, E., 2013. Constant dimensionality of fault roughness from the scale of micro-fractures to the scale of continents. Geophysical Research Letters 40, 83–87. https://doi.org/10.1029/2012GL054143
Renard, F., Voisin, C., Marsan, D., Schmittbuhl, J., 2006. High resolution 3D laser scanner measurements of a strike-slip fault quantify its morphological anisotropy at all scales. Geophysical Research Letters 33. https://doi.org/10.1029/2005GL025038
Rockwell, T.K., Klinger, Y., 2013. Surface rupture and slip distribution of the 1940 Imperial Valley earthquake, Imperial fault, Southern California: Implications for rupture segmentation and dynamics. Bulletin of the Seismological Society of America 103, 629–640. https://doi.org/10.1785/0120120192
Roy, A., Roy, N., Saha, P., & Mandal, N., 2021. Factors Determining Shear-Parallel Versus Low-Angle Shear Band Localization in Shear Deformations: Laboratory Experiments and Numerical Simulations. Journal of Geophysical Research: Solid Earth, 126, e2021JB022578. https://doi.org/10.1029/2021JB022578
Rubin, A.M., Gillard, D., Got, J.-L., 1999. Streaks of microearthquakes along creeping faults. Nature 400, 635–641. https://doi.org/10.1038/23196
Sagy, A., Brodsky, E.E., 2009. Geometric and theological asperities in an exposed fault zone. Journal of Geophysical Research: Solid Earth 114. https://doi.org/10.1029/2008JB005701
Sagy, A., Brodsky, E.E., Axen, G.J., 2007. Evolution of fault-surface roughness with slip. Geology 35, 283–286. https://doi.org/10.1130/G23235A.1
Saha, A.K., 1994. Crustal evolution of Singhbhum-North Orissa, Eastern India. Geological Society of India.
Schmittbuhl, J., Chambon, G., Hansen, A., Bouchon, M., 2006. Are stress distributions along faults the signature of asperity squeeze? Geophysical Research Letters 33. https://doi.org/10.1029/2006GL025952
Schmittbuhl, J., Gentier, S., Roux, S., 1993. Field Measurements of the Roughness of Fault Surfaces. Geophysical Research Letters 20, 639–641. https://doi.org/10.1029/93GL00170
Scholz, C.H., Aviles, C.A., 1986. The fractal geometry of faults and faulting. pp. 147–155. https://doi.org/10.1029/gm037p0147
Scholz CH, Campos J. The seismic coupling of subduction zones revisited. J Geophys Res Solid Earth. 2012;117(5). doi:10.1029/2011JB009003
Sengupta, S., Ghosh, S.K., 1997. The kinematic history of the Singhbhum shear zone. Proceedings of the Indian Academy of Sciences-Earth and Planetary Sciences 106, 185–196.
Sibson, R.H., 2003. Brittle-failure controls on maximum sustainable overpressure in different tectonic regimes. American Association of Petroleum Geologists Bulletin 87, 901–908. https://doi.org/10.1306/01290300181
Sibson, R.H., 1977. Fault rocks and fault mechanisms. Journal of the Geological Society 133, 191–213. https://doi.org/10.1144/ gsjgs.133.3.0191
Turcotte, D.L., 1997. Fractals and chaos in geology and geophysics, 2nd ed. Cambridge University Press, Cambridge, UK. https://doi.org/https://doi.org/10.1017/ CBO9781139174695
Twiss, R.J., Moores, E.M., 1992. Structural Geology-W. H. Freeman (1992). W. H. Freeman Publications, New York.
Voisin, C., 2002. Dynamic triggering of earthquakes: The nonlinear slip-dependent friction case. Journal of Geophysical Research: Solid Earth 107, ESE 10-1-ESE 10-11. https://doi.org/10.1029/2001jb001121
Voisin, C., Campillo, M., Ionescu, I., Hassani, R., Nguyen, Q.-L., 2002. Process and signature of initiation on a finite fault system: a spectral approach. Geophysical Journal International 148, 120–131. https://doi.org/10.1046/j.1365-246x.2002.01571.x
Wells, D.L., Coppersmith, K.J., 1994. New empirical relationships among magnitude, rupture length, rupture width, rupture area, and surface displacement. Bulletin of the Seismological Society of America 84, 974–1002. https://doi.org/10.1785/BSSA0840040974
Zeng, Y., Anderson, J., 2000. Evaluation of numerical procedures for simulating near-fault long-period ground motions using Zeng method. Report 2000/01 to the PEER Utilities Program. http://peer.berkeley.edu
Zimmerman, R.W., Bodvarsson, G.S., 1996. Hydraulic conductivity of rock fractures. Transport in Porous Media. 23, 1–30. https://doi.org/https://doi.org/10.1007/BF00145263